PHYSICAL REVIEW B **108**, 235132 (2023)

Dynamical exchange-correlation potential formalism for spin-$\frac{1}{2}$ Heisenberg and Hubbard chains: The antiferromagnetic/half-filled case

Zhen Zhao[1,*] Claudio Verdozzi[1,†] and Ferdi Aryasetiawan[1,2,‡]
[1]*Division of Mathematical Physics and ETSF, Lund University, P.O. Box 118, 221 00 Lund, Sweden*
[2]*LINXS Institute of advanced Neutron and X-ray Science (LINXS), IDEON Building Delta 5, Scheelevägen 19, 223 70 Lund, Sweden*

(Received 25 May 2023; accepted 20 November 2023; published 11 December 2023)

The exchange-correlation potential formalism previously introduced and applied to the one-dimensional Hubbard model has been extended to spin systems and applied to the case of the one-dimensional antiferromagnetic spin-$\frac{1}{2}$ Heisenberg model. Within the spin exchange-correlation potential formulation, a sum rule for spin systems is derived. The exchange-correlation potential for the Heisenberg model is extrapolated from exact diagonalization results of small antiferromagnetic Heisenberg clusters. This procedure is also employed to revisit and computationally improve the previous investigation of the exchange-correlation potential of the half-filled Hubbard model, which was based on the exchange-correlation potential of the dimer. Numerical comparisons with exact benchmark calculations for both the Heisenberg and the Hubbard models indicate that, starting from the exchange-correlation potential of a finite cluster, the extrapolation procedure yields a one-particle spectral function with favorable accuracy at a relatively low computational cost. In addition, a comparison between the ground-state energies for the one-dimensional Hubbard and Heisenberg models displays how the well-known similarity in behavior of the two models at large interactions manifests itself within the exchange-correlation potential formalism.

DOI: 10.1103/PhysRevB.108.235132

I. INTRODUCTION

Lattice models, in spite of their apparent simplicity, can be very valuable to reveal important features in low-dimensional and highly correlated quantum systems. This certainly is the case of two highly paradigmatic models of condensed matter physics, namely the Hubbard [1] and spin-$\frac{1}{2}$ quantum Heisenberg models [2].

For several decades, these two models have been a test ground for new theoretical and computational methods [3–5]. Notably, they have been used to describe phenomena such as the Mott transition [6], high-critical-temperature superconductivity [7], quantum spin liquids [8], and quantum entanglement [9,10]. Furthermore, via suitable parametrization from first-principles ground-state calculations, they have also been used to describe the dynamical behavior of real materials, which is experimentally measurable via, e.g., neutron scattering and angle-resolved photoemission spectroscopy. This model approach is very useful when first-principles descriptions are too complicated to perform (see, e.g., Refs. [11–14]).

There are a number of approaches of increasing sophistication being continuously developed to solve the Hubbard and Heisenberg models [15–22]. Exact analytical solutions remain scarce. In one dimension (1D), both models are integrable and exactly solvable via the Bethe ansatz [23,24]. Yet, exact analytic treatments for higher-dimensional or even extended 1D systems [e.g., with next-nearest-neighbor (NNN) coupling] are in general not available. As it happens, already in 1D not all quantities of interest can be accessed: The Bethe ansatz provides information about the energy dispersion [25,26] but not, for example, the spectral weight, one of the more interesting quantities to consider when studying dynamical correlations (the latter are usually directly connected to experimental results). In this case, approaches based on the Bethe ansatz, such as the vertex-operator approach [27] or the algebraic Bethe ansatz [28,29], have been used.

On the numerical side, several approaches can be suitably employed for both models, such as exact diagonalization (ED) [30], quantum Monte Carlo (QMC) [31–34], and density matrix renormalization group (DMRG) [35–37], to name a few. ED gives exact and complete information about the system, but it is restricted to small systems and thus is unable to capture the thermodynamic limit features. DMRG and QMC are applicable to fairly large systems and have high accuracy in 1D [38–40], but for higher dimensions the computational cost increases rapidly [41–43].

Density functional theory (DFT) [44–48], a standard methodology for first-principles treatment of materials, has also been used to study the two models [49], via direct adaptation and application of the lattice case [50–54], not only

---

[*] Zhen.Zhao@teorfys.lu.se
[†] Claudio.Verdozzi@teorfys.lu.se
[‡] Ferdi.Aryasetiawan@teorfys.lu.se

to calculate the model parameters from first principles (e.g., Hubbard U [55–57] and Heisenberg J [58]), but also to use model results as input in realistic calculations [59]. Although formally exact, DFT in practice requires approximations for the exchange-correlation energy [60].

The local-density approximation (LDA) and its extension to the local-spin-density approximation (LSDA) are widely used in DFT [47,61,62]. L(S)DA successfully describes many materials but does not perform well in strongly correlated systems, and much effort has been devoted to improving it. With focus on model lattice systems, one way is to use the exact Bethe ansatz solution of the Hubbard model to approximate the correlation energy of an inhomogeneous lattice system [63]. A similar employment of DFT has also been considered for the Heisenberg model [64]. What is noteworthy about these L(S)DA approaches when applied to the Hubbard and Heisenberg models is that the exchange-correlation term has information about the lattice structure and dimensionality of the system.

From a different perspective, a formalism based on the dynamical exchange-correlation potential (Vxc) was recently introduced [65]. The Vxc can be interpreted as the Coulomb potential of the exchange-correlation hole, which represents the density fluctuations in the many-electron system upon addition of a hole or an electron into the system. The formalism is not limited by system size, system dimensionality, or type and range of the interaction, and it is thus useful to describe electronic and magnetic structures in general situations. A main feature of the dynamical Vxc formulation is that the coupling between the dynamical Vxc and the Green's function occurs as a direct product in space and time. In contrast, the self-energy, which is traditionally used to calculate the Green's function, acts on the Green's function as a convolution in space and time.

As a first application of the framework, the lattice one-particle Green's function of the infinite 1D Hubbard chain was determined [65,66] using an extrapolation scheme, starting from the dynamical Vxc of the Hubbard dimer as input. In spite of the simplicity of the approximation used and the low computational load, the scheme provides estimates of the band gap and spectral function in favorable agreement with the results obtained from the Bethe ansatz and the dynamical density matrix renormalization group (DDMRG) [67]. One general conclusion from this investigation is that the Vxc formalism provides a simple picture of the one-electron spectrum: For a given momentum, a time-independent term in the Vxc together with the kinetic energy term determines the main peak of the spectral function, while a time-dependent term in the form of an exponential couples the Green's functions with different momenta and generates incoherent structures or satellite peaks. The energy variable appearing in the exponent can be understood as the main bosonic excitations of the system.

More recently, as a step towards the study of realistic systems, the Vxc of the homogeneous electron gas was calculated within the random-phase approximation [68] with the long-term aim of constructing the Vxc as a universal functional of the ground-state density within the local-density approximation.

II. THIS WORK, AND PLAN OF THE PAPER

In this paper, the Vxc framework is extended to spin systems, more specifically to the 1D Heisenberg model. The Vxc-based equation of motion and the sum rule for the spin exchange-correlation hole are derived. Furthermore, the extrapolation scheme employed in the previous work for the 1D Hubbard chain is adopted [66]. The essential idea of the extrapolation scheme is to start from the Vxc of a finite cluster (kernel), which can be calculated accurately using an exact diagonalization method or other methods such as the density matrix renormalization group. By a suitable extrapolation, this is then used to determine the Green's function of the corresponding lattice model. The spin Vxc framework within the extrapolation scheme is applied to calculate the spectral functions of the 1D spin-$\frac{1}{2}$ antiferromagnetic (AFM) Heisenberg model in the thermodynamic limit, starting from the spin Vxc of small clusters.

In addition, the 1D Hubbard chain is revisited. In the previous work [66], the Hubbard dimer was the kernel, which was used to calculate the Green's function of the 1D Hubbard chain. In this paper, in order to improve the quality of the starting Vxc, the cluster size is enlarged so that additional information arising from interactions beyond nearest neighbors is captured. The improved Vxc is then used to calculate the Green's function of the half-filled 1D Hubbard chain.

To summarize, the main outcomes of the present work are as follows: (i) derivation of the Vxc-based equation of motion and the sum rule of the spin exchange-correlation hole for the 1D Heisenberg model, which can be readily generalized to other spin systems; (ii) calculations of the spinon Green's function for the 1D AFM Heisenberg lattice by extrapolating from a finite-cluster spinon Vxc; (iii) improved treatment of the Vxc of the half-filled 1D Hubbard lattice from the previous work [66] by using as kernel a Vxc from a finite cluster; and (iv) illustration of how in the Vxc formalism the well-known large-U limit (where results from the Hubbard model match those from the AFM Heisenberg one) is recovered.

The plan of the paper is as follows: In Sec. III, we review briefly the general Vxc formalism. Then, in Secs. III A and III B we extend and apply the approach to the 1D AFM Heisenberg model. Specifically, in Secs. III C and III D, we derive an analytic expression for the Vxc for a four-site chain and compute the lattice dynamical structure factor by extrapolating the finite-cluster Vxc to the infinite case. In Sec. IV, we revisit the 1D Hubbard model and compute the exact Vxc of a finite cluster larger than the dimer, with which we improve previous results in the infinite-chain limit. In Sec. V we discuss the Vxc from a comparative perspective, addressing the ground-state energy for both the 1D AFM Heisenberg model and the half-filled 1D Hubbard model in the large-U limit. Finally, in Sec. VI we provide some concluding remarks and an outlook.

III. GENERAL FORMALISM AND APPLICATION TO THE HEISENBERG CHAIN

For a system with a one-body term $h^0(r) = -\frac{1}{2}\nabla^2 + V^{\text{ext}}(r)$ and two-body interactions v, the Hamiltonian reads

$$\hat{H} = \int dr \hat{\psi}^\dagger(r) h^0(r) \hat{\psi}(r) + \frac{1}{2}\int dr_1 dr_2 \hat{\psi}^\dagger(r_1) \times \hat{\psi}^\dagger(r_2) v(r_1, r_2) \hat{\psi}(r_2) \hat{\psi}(r_1), \tag{1}$$

where $\hat{\psi}(r)$ is the fermion field operator and $r = (\mathbf{r}, \sigma)$ is a combined space and spin variable. The time-ordered Green's function is defined in the Heisenberg picture as

$$iG(1,2) := \langle \mathcal{T}\hat{\psi}(1)\hat{\psi}^\dagger(2)\rangle, \tag{2}$$

where the argument numbers label the space-time $1 := (r_1, t_1)$, $\langle\cdot\rangle$ denotes the zero-temperature ground-state expectation value, and $\mathcal{T}$ is the time-ordering symbol. The equation of motion in the Vxc formalism is given by [65]

$$\left[i\partial_{t_1} - h(r_1) - V^{\mathrm{xc}}(1,2)\right] G(1,2) = \delta(1-2), \tag{3}$$

where the single-particle term

$$h(r) = h^0(r) + V^{\mathrm{H}}(r) \tag{4}$$

contains the Hartree potential

$$V^{\mathrm{H}}(r) = \int dr' v(r, r') \rho(r'); \tag{5}$$

$\rho(r)$ is the ground-state electron density. For an equilibrium system, V^{xc} and G depend on the time difference $t_1 - t_2$, and t_2 can be set to zero. The exchange-correlation field has a simple physical interpretation as the Coulomb potential of the exchange-correlation hole ρ^{xc}:

$$V^{\mathrm{xc}}(r, r'; t) = \int dr'' v(r - r'') \rho^{\mathrm{xc}}(r, r', r''; t). \tag{6}$$

The exchange-correlation hole fulfills a sum rule

$$\int d^3 r'' \rho^{\mathrm{xc}}(r, r', r''; t) = -\delta_{\sigma\sigma''}\theta(-t) \tag{7}$$

and an exact constraint

$$\rho^{\mathrm{xc}}(r, r', r'' = r; t) = -\rho(r) \tag{8}$$

for any r, r', and t.

The Vxc reproduces the interaction term containing a special case of the two-particle Green's function, i.e.,

$$V^{\mathrm{xc}}(1,2) iG(1,2) = \int d3 v(1,3) \langle \mathcal{T}\hat{\psi}^\dagger(3)\hat{\psi}(3)\hat{\psi}(1)\hat{\psi}^\dagger(2)\rangle - V^{\mathrm{H}}(1) iG(1,2). \tag{9}$$

For fermion field operators and in the presence of Coulomb interactions, the bare exchange part of the Vxc can be obtained by considering the lowest order of the first term on the right-hand side of Eq. (9),

$$V^{\mathrm{x}}(1,2) iG(1,2) = -\int d3 v(1-3) G(1,3) G(3,2). \tag{10}$$

A. Spin-spin interactions

We now apply the general formalism to spin systems on a discrete lattice. The lattice contains in total N sites, which are labeled with $p = 1, 2, 3, \ldots, N$. At each site, a localized electron orbital gives rise to a local spin. The spin field operators can be written as

$$\hat{S}_p^\alpha = \sum_{\xi\xi'} \hat{c}^\dagger_{p,\xi} \boldsymbol{\sigma}^\alpha_{\xi\xi'} \hat{c}_{p,\xi'}, \tag{11}$$

where $\alpha = x, y, z$ is the spin orientation, $\hat{c}^\dagger_{p,\xi}$ ($\hat{c}_{p,\xi}$) is the creation (annihilation) operator of an electron with spin $\xi = \uparrow, \downarrow$ at site p, and $\boldsymbol{\sigma}^{x,y,z}$ denote the Pauli spin matrices. In what follows, we also use the spin ladder operators: $\hat{S}_p^\pm := \hat{S}_p^x \pm i\hat{S}_p^y$.

For systems with spin-spin interactions, an observable of central interest is the spin dynamical structure factor, whose longitudinal and transverse terms are

$$S^{zz}(k, \omega) = \frac{1}{N}\sum_{pq}\int dt \langle \hat{S}_p^z(t)\hat{S}_q^z(0)\rangle e^{i\omega t} e^{-ik(p-q)} \tag{12}$$

and

$$S^{+-}(k, \omega) = \frac{1}{N}\sum_{pq}\int dt \langle \hat{S}_p^+(t)\hat{S}_q^-(0)\rangle e^{i\omega t} e^{-ik(p-q)}, \tag{13}$$

respectively, where $\hat{S}_p^{z,+,-}(t)$ are the spin field operators in the Heisenberg picture. Also, the time of $\hat{S}_q^{z,-}$ is set to zero, since the system is at equilibrium.

For the Hubbard model, the spin dynamical structure factor can be obtained by solving a two-particle Green's function

$$G^{(2)}_{ppqq}(t) := \langle \mathcal{T}[\hat{c}^\dagger_{p\uparrow}(t)\hat{c}_{p\downarrow}(t)][\hat{c}^\dagger_{q\downarrow}\hat{c}_{q\uparrow}]\rangle, \tag{14}$$

but the equation of motion of the two-particle Green's function contains the three-particle Green's function and thus is generally difficult to solve. Simplification is, however, recovered for large repulsion, where charge transfer becomes less likely and spin correlations can be obtained by studying the AFM Heisenberg model. It is thus of fundamental and practical interest to discuss the Vxc formalism directly for the Heisenberg model.

The isotropic 1D Heisenberg Hamiltonian with nearest-neighbor (NN) exchange coupling is given by

$$\hat{H}^{\mathrm{Heis}} = -J\sum_p \left[\frac{1}{2}(\hat{S}_p^+\hat{S}_{p+1}^- + \mathrm{H.c.}) + \hat{S}_p^z\hat{S}_{p+1}^z\right], \tag{15}$$

where for convenience we use an even total number of sites before taking the thermodynamic limit. We define the Green's function with spin field operators

$$iG_{pq}(t) = \theta(t)\langle \hat{S}_p^+(t)\hat{S}_q^-(0)\rangle + \theta(-t)\langle \hat{S}_q^-(0)\hat{S}_p^+(t)\rangle, \tag{16}$$

in which the Heisenberg J is the analog of the two-particle interaction in Eq. (1). From the Heisenberg equation of motion for the spin field operators, the equation of motion of the Green's function reads

$$i\partial_t G_{pq}(t) + iF_{pq}(t) = 2\delta_{pq}\delta(t)\langle \hat{S}_p^z\rangle, \tag{17}$$

where the interaction term is

$$F_{pq}(t) = -\sum_l J_{pl}[\langle p, l; q\rangle - \langle l, p; q\rangle]. \tag{18}$$

Here,

$$\langle l, p; q\rangle := \langle \mathcal{T}\hat{S}_l^z(t^+)\hat{S}_p^+(t)\hat{S}_q^-(0)\rangle, \tag{19}$$

and $J_{pl} = J(\delta_{l,p+1} + \delta_{l,p-1})$ for the 1D NN exchange coupling. One can define the spin exchange-correlation potential analogous to the charge case as follows:

$$V^{\mathrm{xc}}_{pp,qq}(t)iG_{pq}(t) := F_{pq}(t) - V^{\mathrm{H}}_{p}iG_{pq}(t) - \sum_{l} V^{\mathrm{F}}_{pl}iG_{lq}(t), \tag{20}$$

where the last two terms on the right-hand side, V^{H} and V^{F}, are the analog of the Hartree and exchange potentials, respectively:

$$V^{\mathrm{H}}_{p}(t) := -\sum_{l} J_{pl}\langle \hat{S}^{z}_{l}\rangle, \tag{21}$$

$$V^{\mathrm{F}}_{pl}(t) := J_{pl}\langle \hat{S}^{z}_{p}\rangle. \tag{22}$$

Consequently, a spin correlator $g_{lpq}(t)$ can be defined such that

$$\langle l, p; q\rangle = iG_{pq}(t)g_{lpq}(t)\langle \hat{S}^{z}_{l}\rangle, \tag{23}$$

while the spin exchange-correlation hole ρ^{xc} is defined as

$$\rho^{\mathrm{xc}}_{lpq}(t)iG_{pq}(t) = -\langle l, p; q\rangle + \langle \hat{S}^{z}_{l}\rangle iG_{pq}(t). \tag{24}$$

Denoting the total z component of the spin by $S^{z} = \sum_{l}\langle \hat{S}^{z}_{l}\rangle$, and observing that

$$\sum_{l}\langle l, p; q\rangle = [\theta(-t) + S^{z}]iG_{pq}(t), \tag{25}$$

we can obtain a sum rule for general spin interactions:

$$\sum_{l}\rho^{\mathrm{xc}}_{lpq}(t) = -\sum_{l}[g_{lpq}(t) - 1]\langle \hat{S}_{l}\rangle = -\theta(-t). \tag{26}$$

The detailed derivation is provided in Appendix B.

In this paper, we consider only the case of AFM coupling: that is, $J < 0$, so that $S^{z} = 0$. In the spin-$\frac{1}{2}$ 1D AFM system, the low-lying excitations are known as spinons [18]. Spinons carry fractional spin and are excited in pairs. The dynamical structure factor, which is defined with two spin operators, is related to two-spinon processes. Therefore we call the Vxc defined in Eq. (20) specifically the two-spinon Vxc. It has been shown that the dynamic structure factor corresponding to two-spinon processes has a lower and an upper boundary [15]:

$$\omega^{\mathrm{lb}}(k) = (-J)\frac{\pi}{2}|\sin k|, \tag{27}$$

$$\omega^{\mathrm{ub}}(k) = (-J)\pi\sin\frac{k}{2}, \tag{28}$$

such that for a given k, only $\omega \in [\omega^{\mathrm{lb}}(k), \omega^{\mathrm{ub}}(k)]$ gives nonzero $S(k,\omega)$. For a translationally invariant system, the Hartree and Fock terms [Eqs. (21) and (22)] vanish, and thus the two-spinon Vxc is then

$$V^{\mathrm{xc}}_{pp,qq}(t)iG_{pq}(t) = -J\sum_{\delta=\pm1}[\langle p, p+\delta; q\rangle - \langle p+\delta, p; q\rangle],$$

with the corresponding exchange term (derived in Appendix B) given by

$$\begin{aligned} F^{\mathrm{x}}_{pq}(t) &:= V^{\mathrm{x}}_{pp,qq}(t)iG_{pq}(t) \\ &= J[G_{p+1,p}(0^{+})G_{pq}(t) + G_{p-1,p}(0^{+})G_{pq}(t) \\ &\quad - G_{p,p+1}(0^{+})G_{p+1,q}(t) - G_{p,p-1}(0^{+})G_{p-1,q}(t)]. \end{aligned} \tag{29}$$

In Sec. III B, we show how to use the exchange term F^{x} to find a reference Vxc, as the starting point to solve the Green's function.

B. The infinite chain

We specialize now the description to the case of the homogeneous infinite Heisenberg chain, where $\langle S^{z}_{p}\rangle \equiv s$ is site independent due to translational symmetry. It is convenient to move to the momentum domain, with the Green's function and V^{xc} defined via the Fourier transform as

$$G(k,t) = \frac{1}{N}\sum_{pq} G_{pq}(t)e^{-ik(p-q)}, \tag{30}$$

$$V^{\mathrm{xc}}(k,t) = \frac{1}{N^{2}}\sum_{pq} V^{\mathrm{xc}}_{pp,qq}(t)e^{-ik(p-q)} \tag{31}$$

and where the equation of motion for the Green's function becomes

$$i\partial_{t}G(k,t) - \sum_{k'} V^{\mathrm{xc}}(k-k',t)G(k',t) = 2s\delta(t). \tag{32}$$

In the momentum representation, the exchange term becomes

$$\begin{aligned} F^{\mathrm{x}}(k,t) &= \frac{4J}{N}G(k,t)\sin\frac{k}{2}\sum_{k'} G(k',0^{+})\sin\left(k' - \frac{k}{2}\right) \\ &= -J\lambda\sin^{2}\frac{k}{2}iG(k,t), \end{aligned} \tag{33}$$

where $iG(k',0^{+})$, the static structure factor, is an even function for $k \in [-\pi,\pi]$. We show in Appendix A that λ is a constant which is independent of k. It can be seen that the exchange term V^{x} of the two-spinon Vxc is static in character:

$$V^{\mathrm{x}}(k) := F^{\mathrm{x}}(k,t)/iG(k,t) = -J\lambda\sin^{2}\frac{k}{2}. \tag{34}$$

Inspired by the time-independent structure of V^{x}, we proceed to separate the full Vxc into a dynamical part, $Z^{\mathrm{sp}}(k,t)$, and a static part, V^{s}, i.e.,

$$\begin{aligned} \sum_{k'} V^{\mathrm{xc}}(k-k',t)G(k',t) &= V^{\mathrm{s}}(k)G(k,t) \\ &\quad + Z^{\mathrm{sp}}(k,t)G(k,t). \end{aligned} \tag{35}$$

In this way, we finally arrive at the solution to the equation of motion (32):

$$G(k,t) = G(k,0^{+})e^{-iV^{\mathrm{s}}t}e^{-i\int_{0}^{t} Z^{\mathrm{sp}}(k,t')dt}. \tag{36}$$

In this expression, the k-dependent static term V^{s} determines the main peak of the spectral function, and the dynamical term $Z^{\mathrm{sp}}(k,t)$ produces the satellite structure. To attain an explicit solution, it is expedient to solve for a reference Green's function by keeping only the static V^{s} term in the equation of motion. Here we use Eq. (27) and choose $V^{\mathrm{s}} = \omega^{\mathrm{lb}}$ such that the simplified reference solution contains the lower boundary of the two-spinon energy dispersion [15]

$$G^{\mathrm{ref}}(k,\omega) = \frac{1}{\omega - (-J)\pi|\sin k|/2}. \tag{37}$$

The complete information from the interaction term F is still contained in the dynamic part $Z^{\mathrm{sp}}(k,t)$, which needs to be described appropriately to solve for the full $G(k,\omega)$.

C. A four-site spin chain

It is useful to start our discussion of the spinon Vxc in finite spin clusters by considering a four-site chain. This is the minimal cluster (with an even number of sites) in which the Vxc is nonzero. Furthermore, it is easy to obtain a compact analytical solution that illustrates qualitatively several features present also in larger clusters (in which our solution is numerical in character). To illustrate the features of the four-site Vxc, we choose one of its diagonal elements as a representative case, namely

$$V^{\mathrm{xc}}_{11,11}(t>0) = -J\,\frac{\left(\frac{(xy+x)(xy+x+2y)}{a_+^2}\right)f_1 + (x^2+x)f_2 + \left(\frac{(xy-3x)(xy-3x+2y-4)}{a_-^2}\right)f_3}{\left(\frac{xy+x+2y}{a_+}\right)^2 f_1 + x^2 f_2 + \left(\frac{xy-3x+2y-4}{a_-}\right)^2 f_3}, \tag{38}$$

where $x = 1+\sqrt{3}$, $y = 1+\sqrt{2}$, $a_\pm = \sqrt{8\pm 4\sqrt{2}}$, and $f_{i=1,2,3}$ are time oscillation factors determined by the difference between the spin excitation energies and the ground-state energy. The full details and the explicit forms are given in Appendix C, together with other elements of the Vxc. It is useful at this point to move from site orbitals $\{\varphi_a\}$ to bondinglike ones $\{\phi_\mu\}$. In analogy to what is done with a Bloch basis (a more detailed and comparative discussion of the Bloch basis and the bondinglike basis can be found in Appendix C), we set $\phi_\mu = \sum_a U_{\mu a}\varphi_a$, $\varphi_a = \sum_\mu U_{a\mu}\phi_\mu$, in which $\mu = A, B, C, D$, $a = 1, 2, 3, 4$, and the U matrix is

$$U = \frac{1}{2}\begin{pmatrix} 1 & 1 & 1 & 1 \\ 1 & -1 & 1 & -1 \\ 1 & 1 & -1 & -1 \\ 1 & -1 & -1 & 1 \end{pmatrix}. \tag{39}$$

For the Green's functions, the transformation reads $G_{\mu\nu} = \sum_{ab} U_{\mu a} G_{ab} U^*_{b\nu}$ and $G_{ab} = \sum_{\mu\nu} U^*_{a\mu} G_{\mu\nu} U_{\nu b}$. One can define

$$V^{\mathrm{xc}}_{\mu\alpha,\beta\nu}(t) := \sum_{mn} U_{\mu m} U^*_{m\alpha} V^{\mathrm{xc}}_{mm,nn}(t) U_{\beta n} U^*_{n\nu}, \tag{40}$$

such that the equation of motion is now

$$i\partial_t G_{\mu\nu}(t) - \sum_{\alpha\beta} V^{\mathrm{xc}}_{\mu\alpha,\beta\nu}(t) G_{\alpha\beta}(t) = s_{\mu\nu}\delta(t), \tag{41}$$

where $s_{\mu\nu} = 2\sum_{pq} U_{\mu p}\langle S^z_p\rangle \delta_{pq} U^*_{q\nu}$. Comparing the equation of motion for the diagonal terms $G_{\mu\mu}$,

$$\left[i\partial_t - V^{\mathrm{xc}}_{\mu\mu,\mu\mu}\right] G_{\mu\mu}(t) - \sum_{\gamma\neq\mu} V^{\mathrm{xc}}_{\mu\gamma,\gamma\mu} G_{\gamma\gamma}$$
$$- \sum_{\gamma\neq\delta} V^{\mathrm{xc}}_{\mu\gamma,\delta\mu}(t) G_{\gamma\delta}(t) = s_{\mu\mu}\delta(t), \tag{42}$$

to the infinite-chain equation of motion (32), we note the following: (i) $G_{\mu\mu}$ maps to $G(k)$; (ii) the contribution from fully off-diagonal terms $V^{\mathrm{xc}}_{\mu\nu,\delta\mu}$ should be negligible; (iii) $V^{\mathrm{xc}}_{\mu\gamma,\gamma\mu}$, which maps to $V(k)$, depends only on the difference of μ, γ; and (iv) the weights of the higher-excitation term f_3 are relatively small.

According to points (i)–(iv) and ignoring the high-energy-excitation contributions from f_3, one thus arrives at an approximate expression for the matrix elements of $V^{xc}_{\mu\gamma,\gamma\mu}$:

$$V^{\mathrm{xc}}_{BB,BB}(t>0) \approx -J\alpha,$$
$$V^{\mathrm{xc}}_{BC,CB}(t>0) \approx -J\beta\exp\left[\frac{iJt}{\sqrt{2}}\right], \tag{43}$$

whereas $V^{\mathrm{xc}}_{BD,DB}(t>0) \approx 0$, $V^{\mathrm{xc}}_{BA,AB}(t>0) \approx 0$, in which

$$\alpha := \frac{xy+x}{xy+x+2y} = \frac{2x+2}{xy+x+2}, \tag{44}$$

$$\beta := \frac{1}{4}\left(\frac{a_+}{xy+x+2y} + \frac{a_+}{xy+x+2}\right)^2 (x^2+x-\alpha x^2), \tag{45}$$

and as in (38), $a_+ = \sqrt{8+4\sqrt{2}}$. The analytic spinon Vxc in the bonding basis and its main excitation approximation are shown in Fig. 1. Ignoring the high-excitation factor f_3 reduces the fine-structure details in Vxc. Consequently, $V^{\mathrm{xc}}_{BB,BB}$ simplifies to a constant whereas $V^{\mathrm{xc}}_{BC,CB}$ oscillates with a single frequency and a constant magnitude, and all other components are negligible.

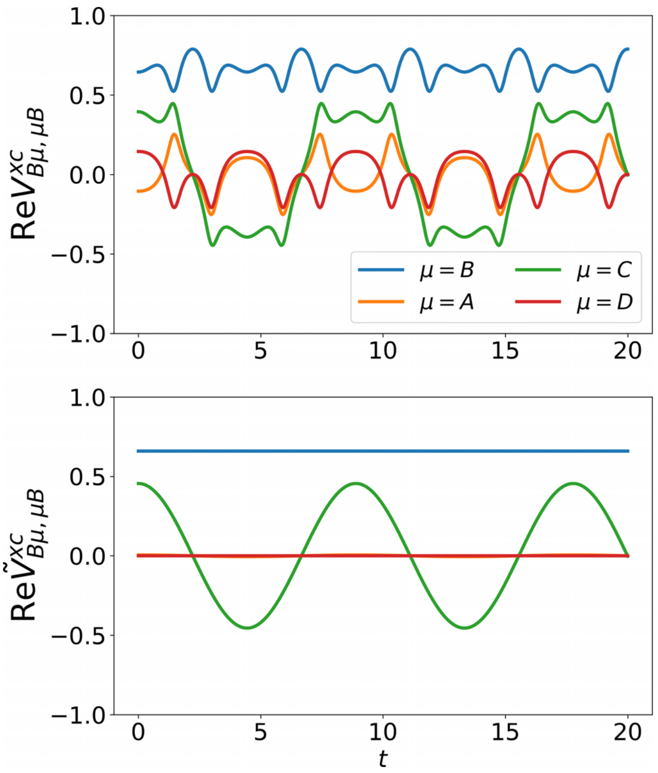

FIG. 1. Real part of the Vxc of a four-site spin-$\frac{1}{2}$ AFM Heisenberg chain, in units of $|J|$. Top: exact. Bottom: results when the high-excitation contribution is ignored [see Eqs. (43)–(45) and related discussion].

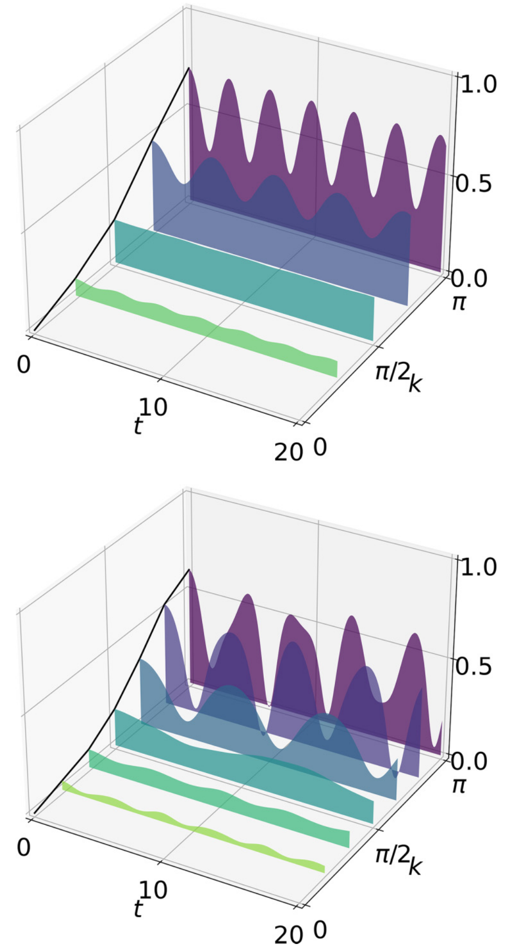

FIG. 2. Real part of Z^{sp} from a spin-$\frac{1}{2}$ AFM Heisenberg ring. Top (bottom): results for a ring with 8 (12) sites.

D. Infinite chain from cluster extrapolation

In Fig. 2, we show $\mathrm{Re}Z^{\mathrm{sp}}(k,t)$ as obtained from the cluster Vxc discussed in the previous section.

It can be seen that for each k, $\mathrm{Re}Z^{\mathrm{sp}}(k,t)$ oscillates in time, a behavior that can be understood as due to a single quasiparticle-like main excitation. We therefore propose the following ansatz for Z^{sp} in the infinite-chain case:

$$Z^{\mathrm{sp}}(k,t)=\mathcal{A}(k)e^{-i\omega^{\mathrm{sp}}(k)t}+\mathcal{B}(k), \tag{46}$$

where the amplitude $\mathcal{A}$, the spinon excitation energy ω^{sp}, and the shift term $\mathcal{B}$ all increase monotonically as k increases from 0 to π. The Green's function is given by inserting the ansatz into Eq. (36):

$$\begin{aligned}&G^{\mathrm{sp}}(k,t>0)\\&\quad=G^{\mathrm{sp}}(k,0^+)e^{-i[V^{\mathrm{s}}(k)+\mathcal{B}(k)]t}e^{\frac{\mathcal{A}(k)}{\omega^{\mathrm{sp}}(k)}(e^{-i\omega^{\mathrm{sp}}(k)t}-1)},\end{aligned} \tag{47}$$

where the static potential is $V^{\mathrm{s}}(k)=-J\pi|\sin k|/2$.

Expanding the last term on the right-hand side of Eq. (47) to first order in $e^{-i\omega^{\mathrm{sp}}(k)t}$, i.e.,

$$e^{\frac{\mathcal{A}(k)}{\omega^{\mathrm{sp}}(k)}(e^{-i\omega^{\mathrm{sp}}(k)t}-1)}\approx 1+\frac{\mathcal{A}(k)}{\omega^{\mathrm{sp}}(k)}(e^{-i\omega^{\mathrm{sp}}(k)t}-1), \tag{48}$$

one gets an approximate Green's function

$$\begin{aligned}G^{\mathrm{sp}}_{(1)}(k,t>0)&=G^{\mathrm{sp}}(k,0^+)e^{-i[V^{\mathrm{s}}(k)+\mathcal{B}(k)]t}\\&\quad\times\left[1+\frac{\mathcal{A}(k)}{\omega^{\mathrm{sp}}(k)}(e^{-i\omega^{\mathrm{sp}}(k)t}-1)\right],\end{aligned} \tag{49}$$

which in the frequency domain becomes

$$\begin{aligned}G^{\mathrm{sp}}_{(1)}(k,\omega)=G^{\mathrm{sp}}(k,0^+)&\left[\frac{1-\frac{\mathcal{A}(k)}{\omega^{\mathrm{sp}}(k)}}{\omega-[V^{\mathrm{s}}(k)+\mathcal{B}(k)]}\right.\\&\left.+\frac{\frac{\mathcal{A}(k)}{\omega^{\mathrm{sp}}(k)}}{\omega-[V^{\mathrm{s}}(k)+\mathcal{B}(k)+\omega^{\mathrm{sp}}(k)]}\right].\end{aligned} \tag{50}$$

From Eq. (50), it can be seen that the main peak position of the dynamical structure factor is given by $V^{\mathrm{s}}+\mathcal{B}$. The spinon excitation energy ω^{sp} transfers weight from the main peak to the higher-energy region resulting in satellite peaks at $V^{\mathrm{s}}+\mathcal{B}+\omega^{\mathrm{sp}}$. The relative weight between the main peak and the satellite is determined by the amplitude term $\mathcal{A}$ and the spinon energy ω^{sp}. Specifically at $k=\pi$, the finite-cluster solution gives nonzero $\mathcal{B}$, which opens a spin gap that does not exist for the spin-$\frac{1}{2}$ lattice. We attribute this to finite-size effects, and thus we adjust $\mathcal{B}$ to a smaller value in our extrapolation.

Based on our discussion so far, we now present the lattice case obtained by extrapolating the cluster Vxc. The 12-site cluster ED result provides $Z^{\mathrm{sp}}(K,t)$ and $G(K,0^+)$ for $K=\frac{2\pi}{12}\times 0,1,2,\ldots,6$ (we only need to consider $0\leqslant K\leqslant\pi$). For each K, we extract $\mathcal{A}(K)$ as half the difference between the maximum and minimum of $\mathrm{Re}Z^{\mathrm{sp}}(K,t)$. We approximate $\omega^{\mathrm{sp}}(K)=2\pi/\bar{T}$, where $\bar{T}$ is the average time difference between neighboring peaks of $\mathrm{Re}Z^{\mathrm{sp}}(K,t)$. To reduce the gap opening due to the finite size, we set $\mathcal{B}(\pi)=0.2$ to be comparable to the broadening factor. For other k values, we estimate $\mathcal{A}(k)$, $\mathcal{B}(k)$, and $G(k,0^+)$ by linear interpolation and estimate the spinon excitation energy by fitting to the two-spinon spectrum boundary,

$$\omega^{\mathrm{sp}}\to(-J)\pi\left[\sin\frac{k}{2}-\frac{1}{2}|\sin k|\right]. \tag{51}$$

The longitudinal and transverse spin dynamical structure factors are then calculated from the spinon Green's function. Since for a spin isotropic system S^{zz} and S^{+-} differ by a constant factor, we only calculate the spectral function of the Green's function [Eq. (47)], as shown in Fig. 3 (interestingly, approximating the term $\exp\{\frac{\mathcal{A}}{\omega^{\mathrm{sp}}}[\exp(-i\omega^{\mathrm{sp}}t)-1]\}$ by $1+\frac{\mathcal{A}}{\omega^{\mathrm{sp}}}[\exp(-i\omega^{\mathrm{sp}}t)-1]$ gives no marked changes of the properties of $G^{\mathrm{sp}}(k,\omega)$). A notable aspect in the behavior of the spin dynamical structure factor is that both the peak locations and the relative weights are close to the inelastic neutron scattering data from the 1D compound $\mathrm{KCuF_3}$ [21] (a DMRG reference result from a 100-site AFM Heisenberg is shown in Appendix A for a qualitative comparison). Coming to more specific features, $S(k,\omega)$ is very small (i.e., close to zero) at small k, while, for a generic k, most of its spectral weight is concentrated around the main peak and the satellite peak. As $k\to\pi$, the relative weight between the main peak and the satellite peak increases, and the spectrum with broadening factor 0.1 is gapless.

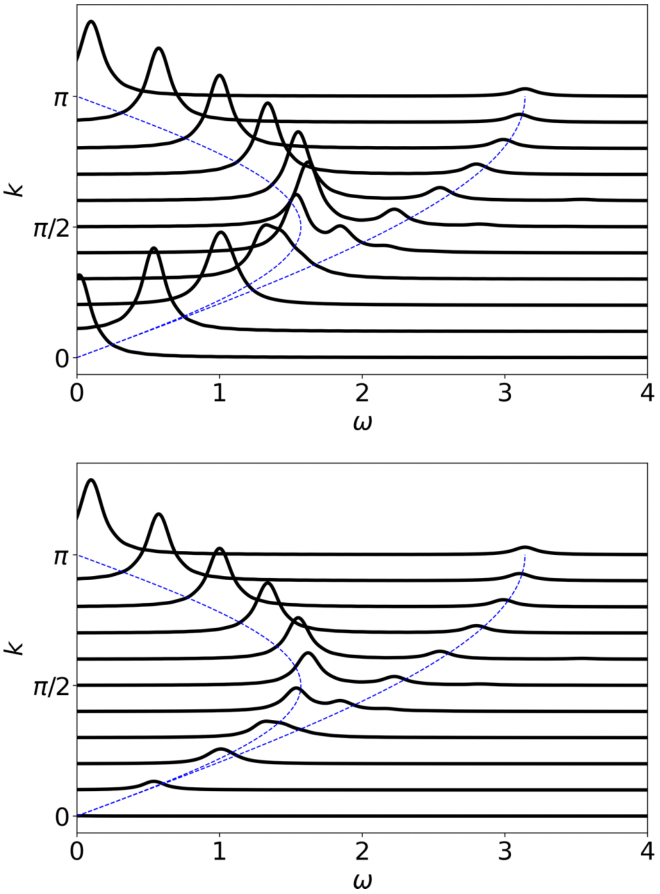

FIG. 3. Dynamic structure factor of a 1D spin-$\frac{1}{2}$ AFM Heisenberg lattice calculated with the Vxc, with broadening 0.1. Top: weight factor $G(k, t = 0)$ considered as the unit. Bottom: weight renormalized with cluster $G(k, 0^+)$. The blue dashed curves are the boundaries for two-spinon processes.

While providing a qualitatively good approximation of the main peak positions and the relative weights of the dynamical structure factor for the 1D AFM Heisenberg model, the present implementation of the spinon Vxc approach is also subject to some limitations. This can be seen by, e.g., comparing the dynamical structure factor from the Vxc approach with the two-spinon lower and upper boundaries (blue dashed curves in Fig. 3). It is apparent that the main peak frequency $\omega = V^{\rm s}(k) + \mathcal{B}$ is still slightly overestimated. To reduce the finite-size effects due to a parameter $\mathcal{B}(\pi)$ originating from a 12-site cluster, we set $\mathcal{B}(\pi)$ to be the same as the broadening factor, i.e., about 0.2 (see Fig. 2). However, the actual Bethe ansatz value of $\mathcal{B}(\pi)$ should be zero. The overall point is that, to obtain a more accurate dynamical structure factor, and to avoid the finite-size effects inherent in the extrapolation from a small cluster, more powerful external methods need to be employed (e.g., the algebraic Bethe ansatz).

These considerations might reveal weaknesses of the extrapolation procedure. However, it must also be clearly stressed that this implementation of the Vxc approach captures most of the qualitative features of the 1D AFM Heisenberg model with a very low computational load and this central attractive feature of the method is expected to also apply in more challenging situations, e.g., in higher dimensions, where rigorous references such as the Bethe ansatz are not available.

IV. IMPROVING THE TREATMENT OF THE 1D HUBBARD LATTICE

Encouraged by the 1D AFM Heisenberg chain results obtained with a Vxc extrapolated from clusters, we now revisit the case of the 1D Hubbard Hamiltonian,

$$\hat{H}^{\rm Hub} = -\Delta \sum_{p\sigma} [\hat{c}^\dagger_{p,\sigma}\hat{c}_{p+1,\sigma} + \text{H.c.}] + U \sum_{p} \hat{n}_{p\uparrow}\hat{n}_{p\downarrow}, \qquad (52)$$

using also in this case a Vxc obtained from small (Hubbard) clusters. In Eq. (52), $p = 1, 2, \ldots, N$ are the site labels (with $N \to \infty$ eventually), $\sigma = \uparrow, \downarrow$ is the spin label, Δ is the hopping energy, and $U > 0$ is the local repulsion. In the site basis, the spin-up channel Green's function is

$$G_{pq}(t) = -i\theta(t)\langle \hat{c}_{p\uparrow}(t)\hat{c}^\dagger_{q\uparrow}(0)\rangle + i\theta(-t)\langle \hat{c}^\dagger_{q\uparrow}(0)\hat{c}_{p\uparrow}(t)\rangle, \qquad (53)$$

and the Vxc reads

$$\begin{aligned} V^{\rm xc}_{pp,qq}(t) iG_{pq}(t) &= U\langle \mathcal{T}\hat{c}^\dagger_{p\downarrow}(t)\hat{c}_{p\downarrow}(t)\hat{c}_{p\uparrow}(t)\hat{c}^\dagger_{q\uparrow}(0)\rangle \\ &\quad - U\rho_{p\downarrow} iG_{pq}(t), \end{aligned} \qquad (54)$$

where $\rho_{p\downarrow}$ is the spin-down particle density at site p. The exchange part of Vxc fulfils

$$V^{\rm x}_{pp,qq}(t) iG_{pq}(t) = -U G_{pp}(0^-) G_{pq}(t), \qquad (55)$$

where $G_{pp}(0^-) = i\langle \hat{c}^\dagger_{p\uparrow}\hat{c}_{p\uparrow}\rangle = i\rho_{p\uparrow}$; thus the exchange part of the Vxc of the Hubbard model is static and cancels the Hartree potential at half filling, in contrast to the Heisenberg model, in which the exchange part depends on the momentum. In general, the exchange part is time dependent [68].

Written in the momentum domain, the equation of motion for the Hubbard lattice takes the form

$$[i\partial_k - \varepsilon_k]G(k, t) - \sum_{k'} V^{\rm xc}(k - k', t)G(k', t) = \delta(t), \qquad (56)$$

where $\varepsilon_k = -2\Delta \cos k$ is the kinetic energy. Equation (56) shows that the interaction term, expressed as the direct product of the Vxc and the Green's function in the space-time domain, is a convolution in the momentum domain. It has been shown [66] that the main peak position of the electron (hole) spectral functions can be described with $V^{\rm xc}(k = 0)$, together with the kinetic energy, while $V^{\rm xc}(k = \pi)$ plays an important role in determining the satellite peaks. One can also write the interaction term as a direct product in the momentum domain,

$$\begin{aligned} &\sum_{k'} V^{\rm xc}(k - k', t)G(k', t) \\ &\quad = V^{\rm xc}(0, t)G(k, t) + Y(k, t)G(k, t), \end{aligned} \qquad (57)$$

which gives explicitly the solution for the Green's function:

$$G(k, t > 0) = G(k, 0^+)e^{-i\varepsilon_k t} e^{-i\int_0^t dt' V^{\rm xc}(0,t')} e^{-i\int_0^t dt' Y(k,t')}, \qquad (58a)$$

$$G(k, t < 0) = G(k, 0^-)e^{-i\varepsilon_k t} e^{i\int_t^0 dt' V^{\rm xc}(0,t')} e^{i\int_t^0 dt' Y(k,t')}. \qquad (58b)$$

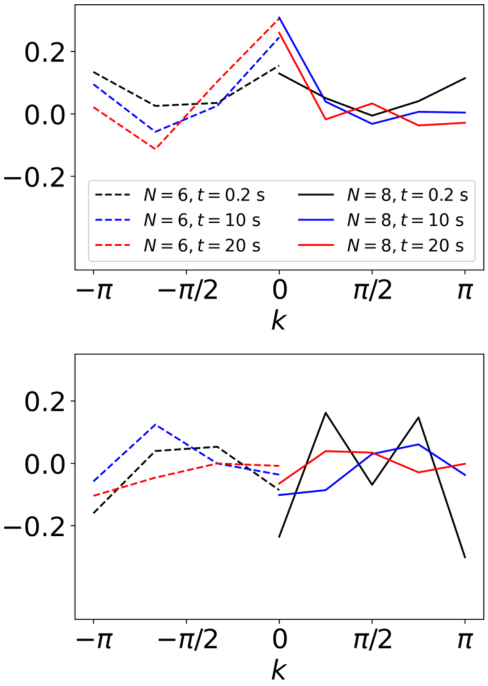

FIG. 4. $V^{\mathrm{xc}}(k)$ of a finite Hubbard ring, $U = 7.74$, $\Delta = 1$, in units of U. Top: real part. Bottom: imaginary part. $V(k,t) = V(-k,t)$, and $V(k,t) = -V(-k,-t)$.

One can then use an N-site cluster with twisted boundary conditions [69] to parametrize $G(k, 0^{\pm})$, and thus the generalized Vxc in the momentum domain becomes

$$Z^{\mathrm{el}}(k,t) := V^{\mathrm{xc}}(0,t) + Y(k,t). \tag{59}$$

Extrapolation from finite clusters

The Vxc of clusters with six and eight sites and with the periodic boundary condition was computed using ED. The Hubbard U was chosen to be 7.74 with $\Delta = 1$, to allow for comparisons with previous work and the DDMRG results from the literature. In contrast to the dimer case, the cluster Vxc exhibits multiple sharp peaks as a function of time t. Time snapshots of the Vxc as a function of k are shown in Fig. 4. For $t \simeq 0$, we have that $V^{\mathrm{xc}}(k,t) \approx V^{\mathrm{xc}}(\pi - k, t)$, but such behavior is unseen during the time evolution. The particle-hole symmetry leads to $V^{\mathrm{xc}}(k,-t) = -V^{\mathrm{xc}}(k,t)$, and the increase of cluster size from $N = 6$ to $N = 8$ does not change qualitatively the characteristics of V^{xc} as a function of k.

The dynamical properties of Vxc can be better illustrated through Z^{el}, a generalization of the Vxc in the momentum basis defined in Eq. (59). Due to degeneracy, $Z^{\mathrm{el}}(-k,t) = Z^{\mathrm{el}}(k,t)$, and because of particle-hole symmetry, $Z^{\mathrm{el}}(k,-t) = -Z^{\mathrm{el}}(\pi - k, t)$. To improve the simulation of Z^{el}, we use a cluster with the twisted boundary condition, which provides larger k-point sampling. The real part of $Z^{\mathrm{el}}(k,t)$ with the twisted boundary condition is shown in Fig. 5: For small k, it oscillates weakly in time (with small amplitude and long period). However, where the band gap opens ($k \to \frac{\pi}{2}$), the oscillation of $\mathrm{Re}Z^{\mathrm{el}}$ is more evident. For $k \to \pi$, $\mathrm{Re}Z^{\mathrm{el}}$ exhibits sharp peaks at certain times. The peaks can be both positive and negative: Mathematically, this means that some of the zeros of the Green's function are located where the interaction term [Eq. (54)] has nonzero finite (positive or negative) values. These spiky structures cannot be fitted into a weighted sum of several (but finite in number) oscillations, indicating that a model beyond the single-energy quasiparticle picture is necessary.

Provided with the numerically exact Vxc for $N = 6$, 8 clusters, we reconsider the approximate scheme proposed in the previous work based on the Hubbard dimer ($N = 2$) [66]. The dimer admits two k points ($k = 0, \pi$), with the corresponding approximate values for the Vxc given by

$$V^{\mathrm{xc}}(k = 0, t) \approx \frac{\alpha U}{2}, \tag{60a}$$

$$V^{\mathrm{xc}}(k = \pi, t) \approx \frac{\alpha U}{2}(1 - \alpha^2)e^{-i2\Delta t}. \tag{60b}$$

Here, the constant α depends only on $\frac{U}{\Delta}$ (the explicit dependence relation is shown in Appendix D together with a summary of the properties of the Vxc obtained from the Hubbard dimer), and 2Δ in the exponential represents the main excitation energy. In what follows, we use Eqs. (60a) and (60b) to compute the hole part of the spectral function, with

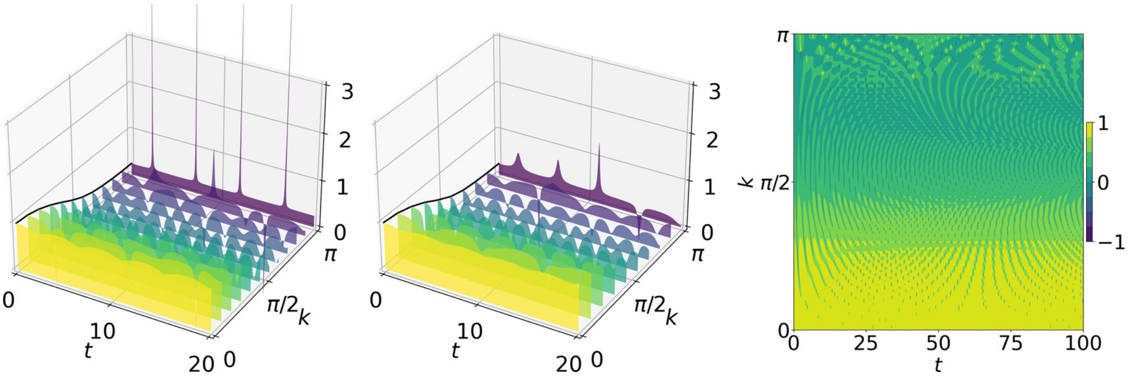

FIG. 5. Real part of $Z^{\mathrm{el}}(k,t)$ of a finite Hubbard chain with the twisted boundary condition, $U = 7.74$, $\Delta = 1$, in units of U. Left and middle: with shorter time scale and fewer k points; $N = 8$, 6, respectively. Right: $N = 6$, with longer time and more k points; peaks out of the color scale are not shown. $Z^{\mathrm{el}}(-k,t) = Z^{\mathrm{el}}(k,t)$, and $Z^{\mathrm{el}}(k,-t) = -Z^{\mathrm{el}}(\pi - k, t)$. For a discussion of the negative peak in the middle panel, see the main text.

the particle part obtainable via the particle-hole symmetry $A^{\mathrm{e}}(k,\omega) = A^{\mathrm{h}}(\pi - k, -\omega)$. When $|k| \leqslant \frac{\pi}{2}$, the hole part of the Green's function given by the dimer model is

$$G^{\mathrm{h}}(k,\omega) = \frac{1}{\omega - \omega_k^{\mathrm{h}} - i\eta}[1 - \mathcal{V}^{xc}(\omega)], \tag{61}$$

$$\mathcal{V}^{xc}(\omega) = \frac{1}{N}\sum_{k'}^{\mathrm{occ}} \frac{V^{\mathrm{xc}}(\pi,0)}{\omega - [\varepsilon_{k'} - V^{\mathrm{xc}}(0) - 2\Delta] - i\eta}, \tag{62}$$

where η is a broadening factor. The spectral function of G^{h} has a main peak at ω_k^{h}, determined by $V^{\mathrm{xc}}(k=0)$ and by the kinetic energy: $\omega_k^{\mathrm{h}} = \varepsilon_k - V^{\mathrm{xc}}(0)$. The term $\mathcal{V}^{xc}(\omega)$ gives rise to a continuous satellite region. Its relative weight to the main peak is $V^{\mathrm{xc}}(\pi,0)$, and its lower and upper boundaries are given by the minimum and maximum occupied state kinetic energy, respectively:

$$\omega_k^{\mathrm{h,lower}} = \varepsilon_0 - V^{\mathrm{xc}}(0) - 2\Delta, \tag{63a}$$

$$\omega_k^{\mathrm{h,upper}} = \varepsilon_{\frac{\pi}{2}} - V^{\mathrm{xc}}(0) - 2\Delta. \tag{63b}$$

The dimer model [66] managed to capture the main structure of the hole spectra of the Hubbard lattice but can be improved in several aspects: The main peak position given by the model is just the kinetic energy $\varepsilon_k = -2\Delta\cos k$ plus a constant determined by U, while the true k dependence of ω^{h} should be more complicated; the upper and lower boundaries of the satellite part given by the model are independent of k, which is also an oversimplification. Rewriting Eq. (58b) in the spirit of a factorization into a main peak term and a satellite term,

$$G(k,t<0) = G(k,0^-)e^{-i(\varepsilon_k + Z_k^{\mathrm{h,main}})t} \times e^{i\int_t^0 dt' Z^{\mathrm{h,sat}}(k,t')}, \tag{64}$$

where $Z_k^{\mathrm{h,main}} + Z^{\mathrm{h,sat}}(k,t) = Z^{\mathrm{el}}(k,t)$ for $t<0$, one can see the following: (i) A momentum-dependent static term, $Z_k^{\mathrm{h,main}}$, which is not present in the dimer model, together with ε_k, determines the main peak; and (ii) the dispersion of $\omega^{\mathrm{h,lower}}$ and $\omega^{\mathrm{h,upper}}$ can be explained by the satellite term $Z^{\mathrm{el,sat}}(k,t')$. Compared with Fig. 5, $Z_k^{\mathrm{h,main}}$ is seen to be the time-independent part around which $Z^{\mathrm{el}}(k,t)$ oscillates, and $Z^{\mathrm{h,sat}}(k,t)$ represents a series of excitation energies. The spikelike $\mathrm{Re}Z^{\mathrm{el}}(k,t)$ for $k \to 0$, $t<0$ is a consequence of multiple excitation energies and large satellite peaks, while the less oscillatory $\mathrm{Re}Z^{\mathrm{el}}(k,t)$ for $k \to \pi$, $t<0$ explains the lack of strong satellites of the hole spectral functions $A^{\mathrm{h}}(k \to \pi, \omega)$.

Taking advantage of the physical picture given by the dimer model, we include the correction to the occupied k values by adding a set of momentum-dependent parameters, $l_{1,2,3}$, such that (i) $\alpha \to \alpha l_1(k)$, (ii) the main excitation determining the satellite boundaries [Eqs. (63a) and (63b)] becomes $2\Delta \to 2\Delta l_2(k)$, and (iii) the effective kinetic energy in the summation of Eq. (61) becomes $\varepsilon_{k'} \to -2\Delta\cos k' l_3(k)$. The parametrized dispersion relations of the key frequencies are

$$\omega_k^{\mathrm{h}} = -2\Delta\cos k - \frac{\alpha U}{2}l_1(k), \tag{65a}$$

$$\omega_k^{\mathrm{h,lower}} = -2\Delta[l_3(k) + l_2(k)] - \frac{\alpha U}{2}l_1(k), \tag{65b}$$

$$\omega_k^{\mathrm{h,upper}} = -2\Delta l_2(k) - \frac{\alpha U}{2}l_1(k). \tag{65c}$$

Thus the hole-part bandwidth for a given momentum, the satellite width, and the band gap are

$$\omega_k^{\mathrm{h}} - \omega_k^{\mathrm{h,lower}} = 2\Delta[l_2(k) + l_3(k) - \cos k], \tag{66a}$$

$$\omega_k^{\mathrm{h,upper}} - \omega_k^{\mathrm{h,lower}} = 2\Delta l_3(k), \tag{66b}$$

$$E_{\mathrm{g}} = \alpha U l_1\left(\frac{\pi}{2}\right), \tag{66c}$$

respectively. This means that the main peak location, the bandwidth, and the satellite region width from cluster calculations can be used to determine the parameters $l_{1,2,3}$, which are then used to calculate the lattice spectral functions $A(k,\omega)$ for $k < \frac{\pi}{2}$. For $k > \frac{\pi}{2}$, where the dimer model gives zero weight for the hole-part spectrum, the cluster results show that the corresponding Vxc can be approximated with a single-energy excitation,

$$Z^{\mathrm{el}}\left(k > \frac{\pi}{2},\ t<0\right) \approx \mathcal{A}_k e^{-i\omega_k^{\mathrm{el}}t} + \mathcal{B}_k, \tag{67}$$

where the parameters $\mathcal{A}$, $\mathcal{B}$, and ω_k^{el} are estimated from cluster result, which is similar to the treatment for the spinon Vxc [Eq. (46)]. Combining the $l_{1,2,3}$-involved occupied region and the $\mathcal{A}$, $\mathcal{B}$, ω^{el}-involved unoccupied region, the hole-part spectral function can now be calculated for the whole Brillouin zone. The spectral functions for selected k values are shown in Fig. 6.

Compared with the dimer model, the cluster Vxc-based parametrization improves the agreement with DDMRG (see, e.g., Figs. 10 and 11 of Ref. [67]) in several aspects. Specifically, we note the following: (i) The missing weights for unoccupied k points appear when using as input a cluster Vxc. (ii) The main peak positions (and thus the band-gap value as well) are more accurate. In fact, the band-gap value from the dimer model, αU, shows a discrepancy with the Bethe ansatz exact value at small U, due to the lack of long-range screening effects. Using a cluster Vxc, however, removes the disagreement. (iii) Both the boundaries and the relative weight of the satellite structure are better described by the cluster Vxc and its momentum-basis generalization Z^{el}. (iv) The total weight of the hole or electron part cannot be renormalized within the dimer model, because the noninteracting Green's function used in the dimer model can only fix the total spectral weight: $\int d\omega A^{\mathrm{h}}(k,\omega) = \theta(k_F - k)$. With a cluster Vxc, using $\langle \hat{c}_k^{\dagger}\hat{c}_k \rangle$, we can rescale the total spectral weight for each k value.

Yet, the main peak ω_k^{h} in Fig. 6 is in general lower than the one from DDMRG. This can be understood as due to the band gap narrowing upon increasing the number of sites (the eight-site cluster we used leads to the overestimation of the gap and thus of the main peak position).

We conclude our discussion of the Hubbard chain by considering its spectral functions in real space that we obtain starting from those in the momentum domain:

$$A(r,\omega) = \frac{1}{2\pi}\int dk A(k,\omega)e^{ikr}, \tag{68}$$

where $r = 0, 1, 2, \ldots$ is in units of the lattice parameter. $A(r,\omega)$ describes the correlation strength between two space points separated by r, at a given energy ω. The local case $A(r=0,\omega)$ corresponds to the density of states.

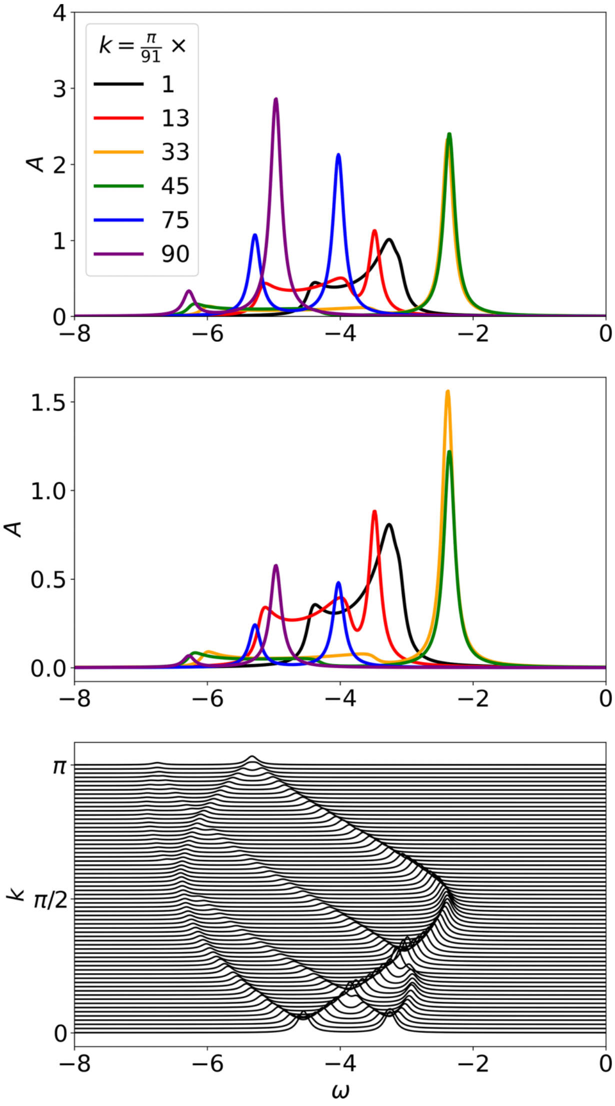

FIG. 6. Momentum-resolved hole-part spectral function $A^{\mathrm{h}}(k, \omega)$ for $U = 7.74$, $\Delta = 1$. For $k < \frac{\pi}{2}$, the parameters $l_{1,2,3}$ are determined using the peak locations of the eight-site twisted boundary condition cluster spectrum. For $k > \frac{\pi}{2}$, Z^{el} of the eight-site twisted boundary condition cluster is used via Eq. (67) to calculate A^{h}. Top (middle): k points chosen to compare with DDMRG results [67], without (with) renormalized weight. Bottom: the satellite structure is approximated with two peaks at the satellite region boundaries, in order to get clearer dispersion branches. The k values are $\frac{\pi}{64} \times 0, 1, 2, \ldots, 64$. The locations of the spinon branch ($0 < k < \pi/2$, $-3.5 < \omega < -2$), the holon branches, and the lower boundary of the holon-spinon continuum ($\pi/2 < k < \pi$, $\omega < -6$) are close to the DDMRG result. For the spinon branch, we have $\omega(k = 0) = -3.25$, which differs from the DDMRG result (approximately equal to -3) because the finite cluster gives in general a larger band gap. In all calculations, we set the broadening parameter $\eta = 0.1$.

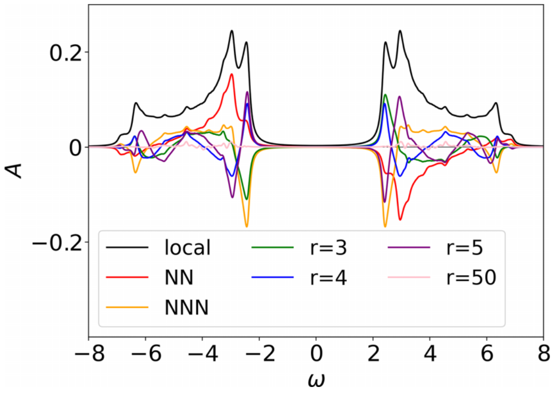

FIG. 7. Spatial spectral functions, calculated with the eight-site Vxc as the kernel (for the six-site case, see Appendix A) for $U = 7.74$, $\Delta = 1$, and broadening $\eta = 0.1$. Sixty-four k points are used to approximate the k integral, according to the Chadi-Cohen method [70].

Results for $A(r, \omega)$ with an eight-site kernel are shown in Fig. 7, while those from a six-site kernel with different U and r are reported in Appendix A. The cluster Vxc result for $A(r = 0, \omega)$ shows better agreement with DDMRG than the dimer model does. Also, the NN spectral weight at positive energy is predominantly negative, and for $r \geqslant 2$, $A(r, \omega)$ exhibits nodal structures. Concerning the role of electronic correlations, spatial spectral functions with different U values become qualitatively alike at large repulsion ($U > 4$), but the band-gap value keeps increasing with U. Finally, spectral functions calculated with eight-site and six-site kernels are qualitatively similar (see Appendix A for the six-site case), with similarities in the overall shape and in the number of nodes. However, the estimated value of the band gap improves upon increasing the cluster size.

V. VXC FROM HUBBARD AND HEISENBERG MODELS: A COMPARATIVE DISCUSSION

It is well known that the 1D spin-$\frac{1}{2}$ AFM Heisenberg model becomes equivalent to the 1D half-filled Hubbard model in the large-U regime [71,72]. After having discussed the Vxc in the two models separately, it can be useful to look at both models together using as perspective the behavior of the Vxc in this limit. Meanwhile, Z^{el} and Z^{sp} do not show a direct asymptotic behavior $Z^{\mathrm{el}}|_{U\to\infty} = Z^{\mathrm{sp}}$, because they are coupled to the single-particle Green's function [Eq. (53)] and single spin-flipping Green's function [Eq. (16)], respectively. For the Hubbard model, the term corresponding to Z^{sp} is coupled to the two-particle Green's function $\langle \mathcal{T}[\hat{c}^{\dagger}_{p\uparrow}(t)\hat{c}_{p\downarrow}(t)][\hat{c}^{\dagger}_{q\downarrow}\hat{c}_{q\uparrow}]\rangle$. The equation of motion of the higher-order Green's function needs to be solved for the Hubbard model to calculate the "higher-order Vxc" that is comparable with the spinon Vxc under large repulsion. This means that the Vxc formalism for the Heisenberg model, having a similar sum rule [Eq. (26)], reduces the difficulty in deriving the equation of motion and improves the interpretability via the quasiparticle picture.

Instead of solving the higher-order Green's function, we consider the more modest task of comparing the lattice ground-state energies for the two models. In the large-U limit [72],

$$\lim_{U\to\infty} \frac{E_0^{\mathrm{Hub}}}{N} = \frac{1}{U}\left(4\frac{E_0^{\mathrm{Heis}}}{N} - 1\right), \tag{69}$$

where E_0^{Hub} is the ground-state energy of an N-site Hubbard ring with $\Delta = 1$ and E_0^{Heis} is the ground-state energy of an

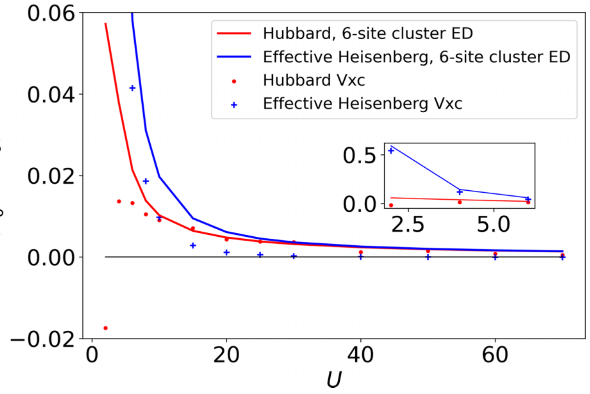

FIG. 8. The ground-state energies calculated with different methods, with the exact Bethe ansatz result for the 1D Hubbard model, $E_0^{\rm BA}$, as a reference. The Vxc-based results for the 1D Hubbard model and the 1D AFM Heisenberg model are indicated with red dots and blue crosses, respectively. The ED results for a six-site Hubbard cluster and a six-site Heisenberg cluster are indicated by red and blue curves, respectively. For both models, the Vxc is extrapolated from a six-site kernel. For Heisenberg model results, Eq. (69) is used.

N-site AFM Heisenberg ring with $J = -1$. Both energies can be calculated from the Green's function via

$$\frac{E_0^{\rm Heis}}{N} = \frac{3}{2}\langle S_1^+(t=0^+)S_2^-\rangle \tag{70}$$

and

$$\frac{E_0^{\rm Hub}}{N} = -[2\langle \hat{c}_{1\uparrow}^\dagger \hat{c}_{2\uparrow}(t=0^-)\rangle - i\partial_t\langle \hat{c}_{1\uparrow}^\dagger \hat{c}_{1\uparrow}(0^-)\rangle]. \tag{71}$$

In the frequency domain,

$$\frac{E_0^{\rm Heis}}{N} = \frac{3i}{4\pi}\int G^{\rm sp}(r=1,\omega)d\omega, \tag{72}$$

$$\frac{E_0^{\rm Hub}}{N} = \frac{i}{2\pi}\int [2G^{\rm el}(r=1,\omega) - \omega G^{\rm el}(r=0,\omega)]d\omega. \tag{73}$$

To perform a comparison, we compute the ground-state energy of the Hubbard lattice in two ways: (i) by directly using the electron Vxc at different U values and (ii) by calculating $E_0^{\rm Heis}$ for a $J = -1$ Heisenberg lattice with the spinon Vxc, to be then used in the effective $E_0^{\rm Hub}$ of Eq. (69). The differences between the results from these two prescriptions and the exact Bethe ansatz solution are shown in Fig. 8. The E_0 results from ED for a six-site ring are also shown as a reference.

For $U < 10$, the repulsion strength is not large enough for Eq. (69) to be valid, leading to a discrepancy between the total energies for the two lattice models. However, in this region, $E_0^{\rm Hub,Vxc}$ (red dots) is already close to the exact Bethe ansatz value, and the difference gets smaller with increasing U. For $U > 30$, the ED results for the two models converge, meaning that the large-repulsion limit is reached. The Vxc-based energies E_0 for the two models also converge to the exact Bethe ansatz value.

It is interesting to observe that the effective Vxc-based Heisenberg result is rather accurate, with an absolute error of less than 10^{-4}: This can be understood as a result of using the two-spinon upper and lower boundaries in the extrapolation and adjusting the $\mathcal{B}$ parameter from the cluster within the zero-spin-gap picture. In contrast, the Vxc-based Hubbard result is extrapolated without a good reference and is more affected by the finite-size effects. Thus the difference between it and the Bethe ansatz result is larger. It could also be that the AFM Heisenberg model does not contain multiple-energy excitations in the two-spinon process. $Z^{\rm sp}$ in the whole Brillouin zone can be described by one ansatz, while $Z^{\rm el}$ has a spikelike structure for certain k, which may suggest that the Vxc for the AFM Heisenberg model as an effective model with no charge flow is simpler than that for the Hubbard model.

As an overall remark, the comparative analysis in this section shows the versatility of the Vxc approach across different lattice models, with results that are consistent with trends and benchmarks from other methods.

VI. CONCLUSION AND OUTLOOK

We have presented an exchange-correlation potential (Vxc) formalism for the one-dimensional antiferromagnetic Heisenberg model and derived a general sum rule for spin systems. Our spin formulation is a tailored extension of a previously introduced general framework for many-body systems that include both charge and spin degrees of freedom. Together with this formulation, we have also devised a procedure to obtain, from a Vxc extracted from small finite clusters, an extrapolation to the thermodynamical limit. This procedure to access the Vxc, originally devised for spin systems, has also permitted us to revisit and improve the treatment of the half-filled one-dimensional Hubbard model, a system already considered in earlier work within the Vxc approach. For both the 1D AFM Heisenberg model and the 1D Hubbard model, the static exchange term of the Vxc was derived and shown to exhibit model-distinctive properties. For the 1D AFM Heisenberg model, the static exchange term corresponds to a dispersion delimited by the boundaries of the two-spinon spectrum, which motivates us to choose the lower boundary as reference. For the Hubbard model, the local U leads to a constant $V^{\rm x}$, which cancels the Hartree potential.

For both models, the spectral functions calculated within the Vxc approach show favorable agreement with DDMRG and with experimental results. Furthermore, a single-energy quasiparticle picture can be used to explain the dynamics of the spinon Vxc for the 1D AFM Heisenberg model and the unoccupied or occupied part of the hole or electron Vxc for the 1D Hubbard model. Finally, we showed how the Vxc formalism captures the equivalence of the two models in the large-U limit, by a comparative analysis via the lattice ground-state energies.

In conclusion, our results indicate that the Vxc formalism provides an alternative way of calculating the single-particle Green's function which is computationally cost-beneficial but also physically well defined. Looking forward, we plan to apply this dimensionality- and interaction-insensitive scheme to models of increasing complication and higher dimensionality. At the same time, we intend to explore ways to devise accurate Vxc approximations with the goal of calculating excited-state properties of real materials from first principles.

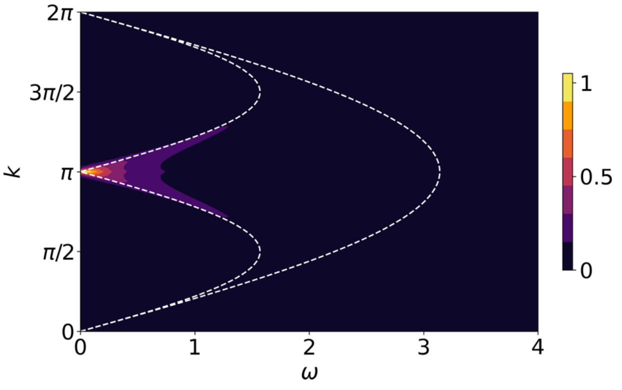

FIG. 9. The dynamic structure factor of a 100-site AFM Heisenberg chain with $J=-1$, computed with DMRG. The weights are renormalized to be in the range 0–1.

ACKNOWLEDGMENTS

F.A. gratefully acknowledges financial support from the Knut and Alice Wallenberg Foundation (Grant No. 2017.0061) and the Swedish Research Council [Vetenskaprådet (VR) Grant No. 2021_04498_3]. C.V. gratefully acknowledges financial support from the Swedish Research Council (VR Grants No. 2017-03945 and No. 2022-04486). Z.Z. gratefully acknowledges financial support from the Swedish Research Council (VR Grant No. 2022-04486).

APPENDIX A: ADDITIONAL RESULTS

In conjunction with the discussion given in Sec. III D, we report in Fig. 9 the DMRG dynamical structure factor of a 100-site AFM Heisenberg chain with $J=-1$. Our result is consistent with that in Fig. 2 of the study from Benthien and Jeckelmann [67]. As an additional result to Fig. 7 in Sec. IV, Fig. 10 shows the spatial spectral functions of a Hubbard chain calculated with a six-site kernel.

APPENDIX B: SUM RULE AND EXCHANGE TERM OF A HEISENBERG CHAIN

We first derive the sum rule for the spinon Vxc formalism. Some essential terms and definitions introduced in the main text are repeated here to ensure readability. The equation of motion of the Green's function for the Heisenberg model is

$$i\partial_t G_{pq}(t) + iF_{pq}(t) = 2\delta_{pq}\delta(t)\langle \hat{S}_p^z\rangle, \tag{B1}$$

where the interaction term is

$$F_{pq}(t) = -J\sum_\delta [\langle p, p+\delta; q\rangle - \langle p+\delta, p; q\rangle], \tag{B2}$$

and

$$\langle l, p; q\rangle := \langle \mathcal{T}\hat{S}_l^z(t^+)\hat{S}_p^+(t)\hat{S}_q^-(0)\rangle \tag{B3}$$

is the three-site correlation. The correlator $g_{lpq}(t)$ and the exchange-correlation hole $\rho_{lpq}^{\mathrm{xc}}(t)$ are defined to fulfill

$$\langle l, p; q\rangle = iG_{pq}(t)g_{lpq}(t)\langle \hat{S}_l^z\rangle, \tag{B4}$$

$$\rho_{lpq}^{\mathrm{xc}}(t)iG_{pq}(t) = -\langle l, p; q\rangle + \langle \hat{S}_l^z\rangle iG_{pq}(t), \tag{B5}$$

$$\rho_{lpq}^{\mathrm{xc}}(t) = -[g_{lpq}(t) - 1]\langle \hat{S}_l^z\rangle. \tag{B6}$$

For $t>0$,

$$\sum_l \langle l, p; q\rangle = S^z iG_{pq}(t), \tag{B7}$$

and for $t<0$,

$$\begin{aligned}\sum_l \langle l, p; q\rangle &= \sum_l \big[\langle \hat{S}_q^-(0)\hat{S}_p^+(t)\hat{S}_l^z(t)\rangle + \langle \hat{S}_q^-(0)\hat{S}_p^+(t)\rangle\delta_{pl}\big]\\ &= (1+S^z)iG_{pq}(t).\end{aligned} \tag{B8}$$

Equations (B7) and (B8) can be written in a compact form as

$$\sum_l \langle l, p; q\rangle = [\theta(-t) + S^z]iG_{pq}(t). \tag{B9}$$

Therefore the correlator fulfills

$$\begin{aligned}\sum_l iG_{pq}(t)[g_{lpq}(t) - 1]\langle \hat{S}_l^z\rangle &= \sum_l \langle l, p; q\rangle - \sum_l \langle \hat{S}_l^z\rangle\\ &= \theta(-t)iG_{pq}(t),\end{aligned} \tag{B10}$$

from which the sum rule can be retrieved:

$$\sum_l \rho_{lpq}^{\mathrm{xc}}(t) = -\theta(-t). \tag{B11}$$

Next, we derive the exchange term of the two-spinon Vxc. We define a vertex function

$$\begin{aligned}\Lambda_{lpq}(t) := &\langle \mathcal{T}\hat{S}_l^z(t^+)\hat{S}_p^+(t)\hat{S}_q^-(t')\rangle\\ &- \langle \hat{S}_l^z(t^+)\rangle iG_{pq}(t).\end{aligned} \tag{B12}$$

The interaction term can be written as

$$\begin{aligned}F_{pq}(t) = -J\big[&\Lambda_{p\bar{p}q}(t) - \Lambda_{\bar{p}pq}(t)\\ &+ \langle \hat{S}_p^z(t^+)\rangle iG_{\bar{p}q}(t) - \langle \hat{S}_{\bar{p}}^z(t^+)\rangle iG_{pq}(t)\big],\end{aligned} \tag{B13}$$

where for simplicity, we write $\bar{p} = p+\delta$ as the NN site of p and drop the summation symbol $\sum_\delta$. According to the definition of the Vxc, we have

$$V_{pp,qq}^{\mathrm{xc}}(t)iG_{pq}(t) = -J[\Lambda_{p\bar{p}q}(t) - \Lambda_{\bar{p}pq}(t)]. \tag{B14}$$

Our aim is to find an approximation of Λ such that we can get an expression for the Vxc. To do that, we use the fact that for local spins, $\hat{S}_p^z = \hat{S}_p^+\hat{S}_p^- - \frac{1}{2}$, and we write the vertex function as

$$\begin{aligned}\Lambda_{lpq}(t) = &\langle \mathcal{T}\hat{S}_l^+(t^+)\hat{S}_l^-(t^+)\hat{S}_p^+(t)\hat{S}_q^-(0)\rangle\\ &- \big[\tfrac{1}{2} + \langle \hat{S}_l^z(t^+)\rangle\big]iG_{pq}(t)\end{aligned} \tag{B15}$$

and approximate the correlation with four spin operators as

$$\begin{aligned}&\langle \mathcal{T}\hat{S}_l^+(t^+)\hat{S}_l^-(t^+)\hat{S}_p^+(t)\hat{S}_q^-(0)\rangle\\ &\quad\approx \langle \hat{S}_l^+(t^+)\hat{S}_l^-(t^+)\rangle\langle \mathcal{T}\hat{S}_p^+(t)\hat{S}_q^-(0)\rangle\\ &\qquad+ \langle \hat{S}_p^+(t^+)\hat{S}_l^-(t^+)\rangle\langle \mathcal{T}\hat{S}_l^+(t)\hat{S}_q^-(0)\rangle,\end{aligned} \tag{B16}$$

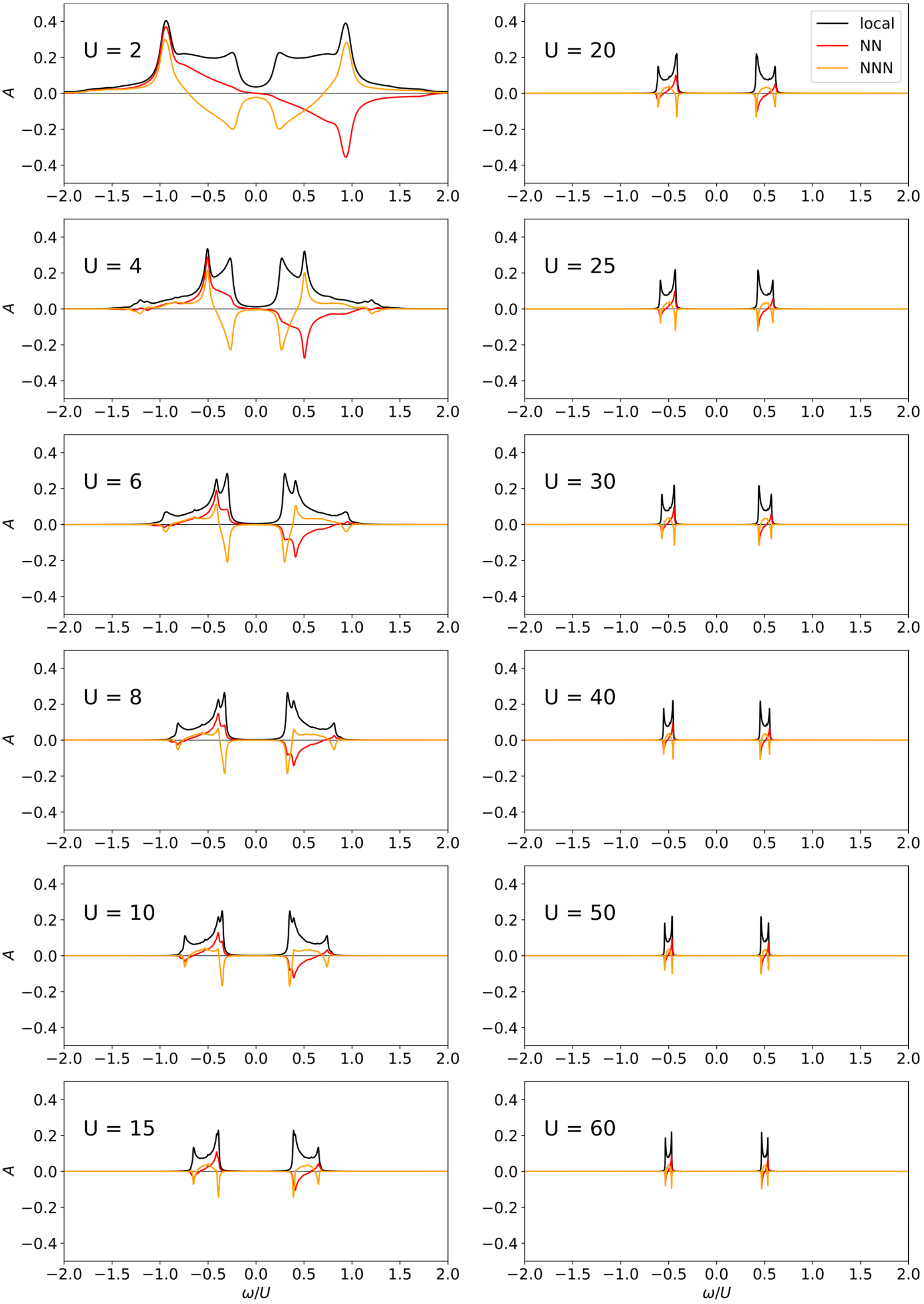

FIG. 10. Spatial spectral functions of a Hubbard chain, calculated with a six-site kernel.

which is a factorization with an exchange of the site indices. Therefore we get the exchange term of the vertex function, which is labeled as Λ^{x}:

$$\Lambda^{\mathrm{x}}_{lpq}(t) := -G_{pl}(0^+)G_{lq}(t). \tag{B17}$$

We also note that $\langle \hat{S}^z_p \rangle = 0$ for AFM Heisenberg lattice; so the exchange part of the interaction term is now

$$\begin{aligned} F^{\mathrm{x}}_{pq}(t) &= -J\left[\Lambda^{\mathrm{x}}_{p\bar{p}q}(t) - \Lambda^{\mathrm{x}}_{\bar{p}pq}(t)\right] \\ &= -J[G_{p,p+1}(0^+)G_{p+1,q}(t) + G_{p,p-1}(0^+)G_{p-1,q}(t) \\ &\quad - G_{p+1,p}(0^+)G_{pq}(t) - G_{p-1,p}(0^+)G_{pq}(t)]. \end{aligned} \tag{B18}$$

This reads in the momentum domain as

$$\begin{aligned} F^{\mathrm{x}}(k,t) &= \frac{-J}{N}\sum_{k'} G(k',0^+)G(k,t) \\ &\quad \times [e^{-ik'}e^{ik} + e^{ik'}e^{-ik} - e^{ik'} - e^{-ik}] \\ &= \frac{-2J}{N}\sum_{k'} G(k',0^+)G(k,t)[\cos(k-k') - \cos(k')] \\ &= \frac{-4J}{N}\sum_{k'} iG(k',0^+)iG(k,t)\sin\frac{k}{2}\sin\left(\frac{k}{2}-k'\right). \end{aligned} \tag{B19}$$

One can notice that the exchange part of the Vxc is time independent:

$$\begin{aligned} V^{\mathrm{s}}(k) &:= \frac{F^{\mathrm{x}}(k,t)}{iG(k,t)} \\ &= \frac{-4J}{N}\sum_{k'} iG(k',0^+)\sin\frac{k}{2}\sin\left(\frac{k}{2}-k'\right), \end{aligned} \tag{B20}$$

which is of even parity for $k \in [-\pi, \pi]$, with $iG(k, 0^+) = \langle S_k^+ S_{-k}^- \rangle$ being the ground-state correlation.

We want to obtain a reference Vxc with F^{x}. Therefore we do not calculate the analytic form of $iG(k, 0^+)$ via the Bethe ansatz, but use the symmetry of $iG(k, 0^+)$ to get an approximate result. We write $iG(k, 0^+)$ as an expansion of even-order polynomials:

$$iG(k,0^+) = \sum_{\xi=0} g_\xi k^{2\xi}. \tag{B21}$$

For the infinite lattice, the finite sum can be replaced with an integral:

$$\begin{aligned} &\frac{1}{N}\sum_{k'} iG(k',0^+)\sin\left(\frac{k}{2}-k'\right) \\ &\to \frac{1}{2\pi}\sum_{\xi} g_\xi \int_{-\pi}^{\pi} dk'(k')^{2\xi}\sin\left(\frac{k}{2}-k'\right). \end{aligned} \tag{B22}$$

In turn, the integral

$$I_\xi(k) := \int_{-\pi}^{\pi} dk'(k')^{2\xi}\sin\left(\frac{k}{2}-k'\right) \tag{B23}$$

can be written as $\sin(\frac{k}{2})$ multiplied with a factor only depending on ξ. Absorbing all the k-independent factors in the expansion coefficient g_ξ, we get

$$V^{\mathrm{s}}(k) = -J\sin^2\frac{k}{2}\left[\frac{1}{\pi}\sum_{\xi} g_\xi\right]. \tag{B24}$$

APPENDIX C: ANALYTIC VXC OF A FOUR-SITE HEISENBERG CHAIN

We start with comparing the Bloch basis, which is usually used for systems with periodicity, and the bondinglike basis, which is defined in Sec. III C for a finite chain with open ends. The Bloch state is defined as $\psi_k = \frac{1}{\sqrt{N}}\sum_a e^{-ika}\varphi_a$. If we write $\tilde{U}_{ka} = \frac{1}{\sqrt{N}}e^{-ika}$, we find that the Bloch basis and the bondinglike basis are transformed similarly from the local orbitals. The difference is that the transformation matrix U is real, while $\tilde{U}$ is complex. We also notice the correspondence between $G(k)$ and $G_{\mu\mu}$,

$$G(k) = \sum_{ab} \tilde{U}_{ka}G_{ab}\tilde{U}^*_{bk}, \tag{C1}$$

$$G_{\mu\mu} = \sum_{ab} U_{\mu a}G_{ab}\tilde{U}^*_{b\mu}, \tag{C2}$$

and between $V^{\mathrm{xc}}(k-k')$ and $V^{\mathrm{xc}}_{\mu\gamma,\gamma\mu}$,

$$V(k-k') = \sum_{ab} \tilde{U}_{ka}\tilde{U}^*_{ak'}G_{ab}\tilde{U}_{k'b}\tilde{U}^*_{bk}, \tag{C3}$$

$$V^{\mathrm{xc}}_{\mu\gamma,\gamma\mu} = \sum_{ab} U_{\mu a}U_{a\gamma}V^{\mathrm{xc}}_{aa,bb}U_{\gamma b}U^*_{b\mu}. \tag{C4}$$

We want to (i) derive the analytic form of the spinon Vxc in the local-orbital basis, (ii) transform the Vxc to the bondinglike basis, and, finally, (iii) with the mapping between the bondinglike basis and the Bloch basis, obtain the features of the lattice Vxc. Therefore, in step (ii), we look at the equation of motion of $G_{\mu\mu}$, which can be mapped to $G(k)$, and ignore terms such as the convolution between $V^{\mathrm{xc}}_{\mu\gamma,\delta\mu}$ and $G_{\gamma\mu}$, since they are numerically small and have no corresponding terms in the Bloch basis. As a result, the Vxc in both the local-orbital basis (labeled by Latin letters) and the bondinglike basis (labeled by Greek letters) can have four indices; however, only $V^{\mathrm{xc}}_{aa,bb}$ and $V^{\mathrm{xc}}_{\mu\gamma,\gamma\mu}$ are considered.

With these manipulations performed, we can then calculate the Green's function in the local-orbital basis. For positive times, we get

$$G_{pq}(t) = \langle\Psi|e^{iHt}\hat{S}^+_p e^{-iHt}\hat{S}^-_q|\Psi\rangle, \tag{C5}$$

where $|\Psi\rangle$ is the ground state. One needs to use a complete set of eigenstates $|n\rangle$ which gives nonzero weight elements $\langle n|\hat{S}^-_q|\Psi\rangle$. For an even number of sites and AFM coupling, the total z spin of $|\Psi\rangle$ is zero, which means that the states $\{|n\rangle\}$ are in the $S^z = -1$ sector. Labeling the eigenenergy corresponding to state $|n\rangle$ with E^-_n, the Green's function can be written as

$$G_{pq}(t>0) = \textstyle\sum_n e^{-i(E^-_n - E^0)t}\langle\Psi|\hat{S}^+_p|n\rangle\langle n|\hat{S}^-_q|\Psi\rangle, \tag{C6}$$

and the interaction term for positive time is

$$\langle l,p;q\rangle_{t>0} = \sum_n e^{-i(E^-_n - E^0)t}\langle\Psi|\hat{S}^z_l\hat{S}^+_p|n\rangle\langle n|\hat{S}^-_q|\Psi\rangle. \tag{C7}$$

By diagonalizing the Hamiltonian in the $S^z = 0$ and $S^z = -1$ sectors, one gets $\{|\Psi\rangle; E^0\}$ and $\{|n\rangle; E^-_n\}$, respectively, and thus the weight elements $\langle n|\hat{S}^-_q|\Psi\rangle$ and $\langle n|\hat{S}^-_p\hat{S}^z_l|\Psi\rangle$, respectively. Out of the four states of $|n\rangle$, only three of them give nonzero $\langle n|\hat{S}^-_q|\Psi\rangle$. Explicitly, the time factors are

$$f_1 = e^{-i(E^-_0 - E^0)t} = e^{iJ(\frac{\sqrt{3}-\sqrt{2}+1}{2})t}, \tag{C8}$$

$$f_2 = e^{-i(E^-_1 - E^0)t} = e^{iJ(\frac{\sqrt{3}+1}{2})t}, \tag{C9}$$

$$f_3 = e^{-i(E^-_2 - E^0)t} = e^{iJ(\frac{\sqrt{3}+\sqrt{2}+1}{2})t}. \tag{C10}$$

The independent elements of V^{xc} in the orbital basis can be calculated with $V^{\mathrm{xc}}_{pp,qq}(t) = \frac{F_{pq}(t)}{iG_{pq}(t)}$:

$$V^{\mathrm{xc}}_{11,11} = -J\frac{\left(\frac{(xy+x)(xy+x+2y)}{a_+^2}\right)f_1 + (x^2+x)f_2 + \left(\frac{(xy-3x)(xy-3x+2y-4)}{a_-^2}\right)f_3}{\left(\frac{xy+x+2y}{a_+}\right)^2 f_1 + x^2 f_2 + \left(\frac{xy-3x+2y-4}{a_-}\right)^2 f_3}, \tag{C11}$$

$$V^{\mathrm{xc}}_{22,22} = -J\frac{\left(\frac{2(x+1)(xy+x+2)}{a_+^2}\right)f_1 + (x^2+x)f_2 + \left(\frac{2(x+1)(xy-3x-2)}{a_-^2}\right)f_3}{\left(\frac{xy+x+2}{a_+}\right)^2 f_1 + x^2 f_2 + \left(\frac{xy-3x-2}{a_-}\right)^2 f_3}, \tag{C12}$$

$$V^{\mathrm{xc}}_{11,22} = -J\frac{\left(-\frac{(xy+x)(xy+x+2)}{a_+^2}\right)f_1 - (x^2+x)f_2 - \left(\frac{(xy-3x)(xy-3x-2)}{a_-^2}\right)f_3}{\left(-\frac{(xy+x+2y)(xy+x+2)}{a_+^2}\right)f_1 - x^2 f_2 - \left(\frac{(xy-3x+2y-4)(xy-3x-2)}{a_-^2}\right)f_3}, \tag{C13}$$

$$V^{\mathrm{xc}}_{11,33} = -J\frac{\left(\frac{(xy+x)(xy+x+2)}{a_+^2}\right)f_1 - (x^2+x)f_2 + \left(\frac{(xy-3x)(xy-3x-2)}{a_-^2}\right)f_3}{\left(\frac{(xy+x+2y)(xy+x+2)}{a_+^2}\right)f_1 - x^2 f_2 + \left(\frac{(xy-3x+2y-4)(xy-3x-2)}{a_-^2}\right)f_3}, \tag{C14}$$

$$V^{\mathrm{xc}}_{11,44} = -J\frac{-\left(\frac{(xy+x)(xy+x+2y)}{a_+^2}\right)f_1 + (x^2+x)f_2 - \left(\frac{(xy-3x)(xy-3x+2y-4)}{a_-^2}\right)f_3}{-\left(\frac{xy+x+2y}{a_+}\right)^2 f_1 + x^2 f_2 - \left(\frac{xy-3x+2y-4}{a_-}\right)^2 f_3}, \tag{C15}$$

$$V^{\mathrm{xc}}_{22,33} = -J\frac{-\left(\frac{2(x+1)(xy+x+2)}{a_+^2}\right)f_1 + (x^2+x)f_2 - \left(\frac{2(x+1)(xy-3x-2)}{a_-^2}\right)f_3}{-\left(\frac{xy+x+2}{a_+}\right)^2 f_1 + x^2 f_2 - \left(\frac{xy-3x-2}{a_-}\right)^2 f_3}, \tag{C16}$$

where the constant factors x, y, and $a_\pm$ are defined in the main text. Other terms such as $V^{\mathrm{xc}}_{33,33}$ can be obtained via considering the symmetry of the chain. The terms in the "bonding-antibonding" basis are then

$$V^{\mathrm{xc}}_{BB,BB} = \frac{1}{16}\left[2\left(V^{\mathrm{xc}}_{11,11} + V^{\mathrm{xc}}_{11,44} + V^{\mathrm{xc}}_{22,22} + V^{\mathrm{xc}}_{22,33}\right) + 4\left(V^{\mathrm{xc}}_{11,22} + V^{\mathrm{xc}}_{11,33}\right)\right], \tag{C17}$$

$$V^{\mathrm{xc}}_{BC,CB} = \frac{1}{16}\left[2\left(V^{\mathrm{xc}}_{11,11} - V^{\mathrm{xc}}_{11,44} + V^{\mathrm{xc}}_{22,22} - V^{\mathrm{xc}}_{22,33}\right) + 4\left(V^{\mathrm{xc}}_{11,22} - V^{\mathrm{xc}}_{11,33}\right)\right], \tag{C18}$$

$$V^{\mathrm{xc}}_{BA,AB} = \frac{1}{16}\left[2\left(V^{\mathrm{xc}}_{11,11} - V^{\mathrm{xc}}_{11,44} + V^{\mathrm{xc}}_{22,22} - V^{\mathrm{xc}}_{22,33}\right) - 4\left(V^{\mathrm{xc}}_{11,22} - V^{\mathrm{xc}}_{11,33}\right)\right], \tag{C19}$$

$$V^{\mathrm{xc}}_{BD,DB} = \frac{1}{16}\left[2\left(V^{\mathrm{xc}}_{11,11} + V^{\mathrm{xc}}_{11,44} + V^{\mathrm{xc}}_{22,22} + V^{\mathrm{xc}}_{22,33}\right) - 4\left(V^{\mathrm{xc}}_{11,22} + V^{\mathrm{xc}}_{11,33}\right)\right]. \tag{C20}$$

APPENDIX D: THE DEPENDENCE OF THE α PARAMETER ON $\frac{U}{\Delta}$ IN THE HUBBARD DIMER MODEL

The equations in this Appendix are rewritten from the Hubbard dimer work [66]. With a two-site open-ends chain, the half-filled Hubbard Hamiltonian equation (52) can be analytically solved, given the analytic bonding ($k = 0$) and antibonding ($k = \pi$) Vxc:

$$V^{\mathrm{xc}}(k=0, t>0) = \frac{\alpha U}{2}\frac{1-\alpha^2 e^{-i4\Delta t}}{1-\alpha^4 e^{-i4\Delta t}}, \tag{D1a}$$

$$V^{\mathrm{xc}}(k=\pi, t>0) = \frac{\alpha U}{2}\frac{(1-\alpha^2)e^{-i2\Delta t}}{1-\alpha^4 e^{-i4\Delta t}}, \tag{D1b}$$

where $\alpha = \frac{1-\kappa}{1+\kappa}$, with $\kappa = \frac{1}{4}\left(\sqrt{(\frac{U}{\Delta})^2 + 16} - \frac{U}{\Delta}\right)$. After neglecting the higher-excitation term $e^{-i4\Delta t}$ in Eq. (D1), the approximated dimer Vxc in the main text [Eq. (60)] is obtained.

---

[1] J. Hubbard, Electron correlations in narrow energy bands, Proc. R. Soc. London, Ser. A **276**, 237 (1963).

[2] W. Heisenberg, Zur Theorie des Ferromagnetismus, Z. Phys. **49**, 619 (1928).

[3] T. Giamarchi, *Quantum Physics in One Dimension*, International Series of Monographs on Physics (Clarendon Press, Oxford, 2004).

[4] F. H. L. Essler, H. Frahm, F. Göhmann, A. Klümper, and V. E. Korepin, *The One-Dimensional Hubbard Model* (Cambridge University Press, Cambridge, 2005).

[5] D. P. Arovas, E. Berg, S. A. Kivelson, and S. Raghu, The Hubbard model, Annu. Rev. Condens. Matter Phys. **13**, 239 (2022).

[6] M. Imada, A. Fujimori, and Y. Tokura, Metal-insulator transitions, Rev. Mod. Phys. **70**, 1039 (1998).

[7] B. Keimer, S. A. Kivelson, M. R. Norman, S. Uchida, and J. Zaanen, From quantum matter to high-temperature superconductivity in copper oxides, Nature (London) **518**, 179 (2015).

[8] L. Savary and L. Balents, Quantum spin liquids: a review, Rep. Prog. Phys. **80**, 016502 (2017).

[9] R. Horodecki, P. Horodecki, M. Horodecki, and K. Horodecki, Quantum entanglement, Rev. Mod. Phys. **81**, 865 (2009).

[10] A. Scheie, P. Laurell, A. M. Samarakoon, B. Lake, S. E. Nagler, G. E. Granroth, S. Okamoto, G. Alvarez, and D. A. Tennant, Witnessing entanglement in quantum magnets using neutron scattering, Phys. Rev. B **103**, 224434 (2021).

[11] N. Motoyama, H. Eisaki, and S. Uchida, Magnetic susceptibility of ideal spin 1/2 Heisenberg antiferromagnetic chain systems, Sr_2CuO_3 and $SrCuO_2$, Phys. Rev. Lett. **76**, 3212 (1996).

[12] D. A. Tennant, T. G. Perring, R. A. Cowley, and S. E. Nagler, Unbound spinons in the S=1/2 antiferromagnetic chain $KCuF_3$, Phys. Rev. Lett. **70**, 4003 (1993).

[13] M. Mourigal, M. Enderle, A. Klöpperpieper, J.-S. Caux, A. Stunault, and H. M. Rønnow, Fractional spinon excitations in the quantum Heisenberg antiferromagnetic chain, Nat. Phys. **9**, 435 (2013).

[14] A. Scheie, P. Laurell, B. Lake, S. E. Nagler, M. B. Stone, J.-S. Caux, and D. A. Tennant, Quantum wake dynamics in Heisenberg antiferromagnetic chains, Nat. Commun. **13**, 5796 (2022).

[15] J. des Cloizeaux and J. J. Pearson, Spin-wave spectrum of the antiferromagnetic linear chain, Phys. Rev. **128**, 2131 (1962).

[16] C. N. Yang and C. P. Yang, One-dimensional chain of anisotropic spin-spin interactions. II. Properties of the ground-state energy per lattice site for an infinite system, Phys. Rev. **150**, 327 (1966).

[17] F. D. M. Haldane, General relation of correlation exponents and spectral properties of one-dimensional Fermi systems: Application to the anisotropic $S = \frac{1}{2}$ Heisenberg chain, Phys. Rev. Lett. **45**, 1358 (1980).

[18] L. Faddeev and L. Takhtajan, What is the spin of a spin wave? Phys. Lett. A **85**, 375 (1981).

[19] G. Müller, H. Thomas, H. Beck, and J. C. Bonner, Quantum spin dynamics of the antiferromagnetic linear chain in zero and nonzero magnetic field, Phys. Rev. B **24**, 1429 (1981).

[20] F. H. L. Essler, V. E. Korepin, and K. Schoutens, Complete solution of the one-dimensional Hubbard model, Phys. Rev. Lett. **67**, 3848 (1991).

[21] B. Lake, D. A. Tennant, J.-S. Caux, T. Barthel, U. Schollwöck, S. E. Nagler, and C. D. Frost, Multispinon continua at zero and finite temperature in a near-ideal Heisenberg chain, Phys. Rev. Lett. **111**, 137205 (2013).

[22] G. H. Booth and G. K.-L. Chan, Spectral functions of strongly correlated extended systems via an exact quantum embedding, Phys. Rev. B **91**, 155107 (2015).

[23] H. Bethe, Zur Theorie der Metalle, Z. Phys. **71**, 205 (1931).

[24] B. S. Shastry, Exact integrability of the one-dimensional Hubbard model, Phys. Rev. Lett. **56**, 2453 (1986).

[25] E. H. Lieb and F. Y. Wu, Absence of Mott transition in an exact solution of the short-range, one-band model in one dimension, Phys. Rev. Lett. **20**, 1445 (1968).

[26] A. A. Ovchinnikov, Excitation spectrum in the one-dimensional Hubbard model, Zh. Eksp. Teor. Fiz. **57**, 2137 (1969) [Sov. Phys. JETP **30**, 1160 (1970)].

[27] J.-S. Caux and R. Hagemans, The four-spinon dynamical structure factor of the Heisenberg chain, J. Stat. Mech. (2006) P12013.

[28] J.-S. Caux, Correlation functions of integrable models: A description of the ABACUS algorithm, J. Math. Phys. **50**, 095214 (2009).

[29] P. Laurell, A. Scheie, D. A. Tennant, S. Okamoto, G. Alvarez, and E. Dagotto, Magnetic excitations, nonclassicality, and quantum wake spin dynamics in the Hubbard chain, Phys. Rev. B **106**, 085110 (2022).

[30] T. Tohyama, P. Horsch, and S. Maekawa, Spin and charge dynamics of the $t - J$ model, Phys. Rev. Lett. **74**, 980 (1995).

[31] M. Suzuki, S. Miyashita, and A. Kuroda, Monte Carlo simulation of quantum spin systems. I, Prog. Theor. Phys. **58**, 1377 (1977).

[32] J. W. Lyklema, Quantum-statistical Monte Carlo method for Heisenberg spins, Phys. Rev. Lett. **49**, 88 (1982).

[33] A. W. Sandvik, A generalization of Handscomb's quantum Monte Carlo scheme-application to the 1D Hubbard model, J. Phys. A: Math. Gen. **25**, 3667 (1992).

[34] M. Raczkowski and F. F. Assaad, Spinon confinement: Dynamics of weakly coupled Hubbard chains, Phys. Rev. B **88**, 085120 (2013).

[35] S. R. White, Density matrix formulation for quantum renormalization groups, Phys. Rev. Lett. **69**, 2863 (1992).

[36] S. R. White, Density-matrix algorithms for quantum renormalization groups, Phys. Rev. B **48**, 10345 (1993).

[37] E. Jeckelmann, Dynamical density-matrix renormalization-group method, Phys. Rev. B **66**, 045114 (2002).

[38] R. Preuss, A. Muramatsu, W. von der Linden, P. Dieterich, F. F. Assaad, and W. Hanke, Spectral properties of the one-dimensional Hubbard model, Phys. Rev. Lett. **73**, 732 (1994).

[39] R. G. Pereira, K. Penc, S. R. White, P. D. Sacramento, and J. M. P. Carmelo, Charge dynamics in half-filled Hubbard chains with finite on-site interaction, Phys. Rev. B **85**, 165132 (2012).

[40] K. Ido, M. Imada, and T. Misawa, Charge dynamics of correlated electrons: Variational description with inclusion of composite fermions, Phys. Rev. B **101**, 075124 (2020).

[41] C. N. Varney, C.-R. Lee, Z. J. Bai, S. Chiesa, M. Jarrell, and R. T. Scalettar, Quantum Monte Carlo study of the two-dimensional fermion Hubbard model, Phys. Rev. B **80**, 075116 (2009).

[42] C. Yang and A. E. Feiguin, Spectral function of the two-dimensional Hubbard model: A density matrix renormalization group plus cluster perturbation theory study, Phys. Rev. B **93**, 081107(R) (2016).

[43] M.-S. Vaezi, A.-R. Negari, A. Moharramipour, and A. Vaezi, Amelioration for the sign problem: An adiabatic quantum Monte Carlo algorithm, Phys. Rev. Lett. **127**, 217003 (2021).

[44] P. Hohenberg and W. Kohn, Inhomogeneous electron gas, Phys. Rev. **136**, B864 (1964).

[45] W. Kohn and L. J. Sham, Self-consistent equations including exchange and correlation effects, Phys. Rev. **140**, A1133 (1965).

[46] E. Runge and E. K. U. Gross, Density-functional theory for time-dependent systems, Phys. Rev. Lett. **52**, 997 (1984).

[47] R. O. Jones and O. Gunnarsson, The density functional formalism, its applications and prospects, Rev. Mod. Phys. **61**, 689 (1989).

[48] G. Onida, L. Reining, and A. Rubio, Electronic excitations: density-functional versus many-body Green's-function approaches, Rev. Mod. Phys. **74**, 601 (2002).

[49] K. Capelle Jr. and V. L. Campo, Density functionals and model Hamiltonians: Pillars of many-particle physics, Phys. Rep. **528**, 91 (2013).

[50] R. López-Sandoval and G. M. Pastor, Interaction-energy functional for lattice density functional theory: Applications to one-, two-, and three-dimensional Hubbard models, Phys. Rev. B **69**, 085101 (2004).

[51] C. Verdozzi, Time-dependent density-functional theory and strongly correlated systems: Insight from numerical studies, Phys. Rev. Lett. **101**, 166401 (2008).

[52] D. Karlsson, A. Privitera, and C. Verdozzi, Time-dependent density-functional theory meets dynamical mean-field theory: Real-time dynamics for the 3D Hubbard model, Phys. Rev. Lett. **106**, 116401 (2011).

[53] D. J. Carrascal, J. Ferrer, J. C. Smith, and K. Burke, The Hubbard dimer: a density functional case study of a many-body problem, J. Phys.: Condens. Matter **27**, 393001 (2015).

[54] M. Qin, T. Schäfer, S. Andergassen, P. Corboz, and E. Gull, The Hubbard model: A computational perspective, Annu. Rev. Condens. Matter Phys. **13**, 275 (2022).

[55] P. H. Dederichs, S. Blügel, R. Zeller, and H. Akai, Ground states of constrained systems: Application to cerium impurities, Phys. Rev. Lett. **53**, 2512 (1984).

[56] O. Gunnarsson, O. K. Andersen, O. Jepsen, and J. Zaanen, Density-functional calculation of the parameters in the Anderson model: Application to Mn in CdTe, Phys. Rev. B **39**, 1708 (1989).

[57] W. E. Pickett, S. C. Erwin, and E. C. Ethridge, Reformulation of the LDA + U method for a local-orbital basis, Phys. Rev. B **58**, 1201 (1998).

[58] I. Rudra, Q. Wu, and T. Van Voorhis, Accurate magnetic exchange couplings in transition-metal complexes from constrained density-functional theory, J. Chem. Phys. **124**, 024103 (2006).

[59] V. I. Anisimov, J. Zaanen, and O. K. Andersen, Band theory and Mott insulators: Hubbard U instead of Stoner I, Phys. Rev. B **44**, 943 (1991).

[60] A. J. Cohen, P. Mori-Sánchez, and W. Yang, Insights into current limitations of density functional theory, Science **321**, 792 (2008).

[61] V. I. Anisimov, F. Aryasetiawan, and A. I. Lichtenstein, First-principles calculations of the electronic structure and spectra of strongly correlated systems: the LDA+U method, J. Phys.: Condens. Matter **9**, 767 (1997).

[62] W. Kohn, Nobel Lecture: Electronic structure of matter–wave functions and density functionals, Rev. Mod. Phys. **71**, 1253 (1999).

[63] N. A. Lima, M. F. Silva, L. N. Oliveira, and K. Capelle, Density functionals not based on the electron gas: Local-density approximation for a Luttinger liquid, Phys. Rev. Lett. **90**, 146402 (2003).

[64] K. Capelle and V. L. Líbero, Spin-density functional theory: Some open problems and application to inhomogeneous Heisenberg models, Int. J. Quantum Chem. **105**, 679 (2005).

[65] F. Aryasetiawan, Time-dependent exchange-correlation potential in lieu of self-energy, Phys. Rev. B **105**, 075106 (2022).

[66] F. Aryasetiawan and T. Sjöstrand, Spectral functions of the half-filled one-dimensional Hubbard chain within the exchange-correlation potential formalism, Phys. Rev. B **106**, 045123 (2022).

[67] H. Benthien and E. Jeckelmann, Spin and charge dynamics of the one-dimensional extended Hubbard model, Phys. Rev. B **75**, 205128 (2007).

[68] K. Karlsson and F. Aryasetiawan, Time-dependent exchange-correlation hole and potential of the electron gas, Phys. Rev. B **107**, 115172 (2023).

[69] B. S. Shastry and B. Sutherland, Twisted boundary conditions and effective mass in Heisenberg-Ising and Hubbard rings, Phys. Rev. Lett. **65**, 243 (1990).

[70] D. J. Chadi and M. L. Cohen, Special points in the Brillouin zone, Phys. Rev. B **8**, 5747 (1973).

[71] P. Fazekas, *Lecture Notes on Electron Correlation and Magnetism* (World Scientific, Singapore, 1999).

[72] W. Nolting and A. Ramakanth, *Quantum Theory of Magnetism* (Springer, New York, 2009).